Palaeogeography, Palaeoclimatology, Palaeoecology 459 (2016) 289–305

Contents lists available at ScienceDirect

Palaeogeography, Palaeoclimatology, Palaeoecology

journal homepage: www.elsevier.com/locate/palaeo

Response of calcareous nannoplankton to the Late Cretaceous Oceanic Anoxic Event 2 at Oued Bahloul (central Tunisia)

Roque Aguado [a,*], Matías Reolid [b], Eustoquio Molina [c]

[a] Departamento de Geología and CEACTierra, Universidad de Jaén, Campus Científico-Tecnológico de Linares, 23700 Jaén, Spain
[b] Departamento de Geología and CEACTierra, Universidad de Jaén, Campus Las Lagunillas, 23071 Jaén, Spain
[c] Departamento de Ciencias de la Tierra and IUCA, Universidad de Zaragoza, Pedro Cerbuna 12, 50009 Zaragoza, Spain

ARTICLE INFO

Article history:
Received 11 April 2016
Received in revised form 10 July 2016
Accepted 12 July 2016
Available online 15 July 2016

Keywords:
Micropalaeontology
Palaeoceanography
Biostratigraphy
Chemostratigraphy
Cenomanian–Turonian

ABSTRACT

Oued Bahloul is a reference section for the Cenomanian–Turonian that was located on the North African palaeomargin, where Oceanic Anoxic Event 2 (OAE2) is represented by black limestones and grey marls. Biostratigraphic study allowed the identification of calcareous nannofossil UC3 to UC6 zones. Quantitative analyses of calcareous nannofossil assemblages indicate that high-fertility surface-water conditions predominated throughout most of the OAE2 interval. The most eutrophic conditions probably developed during deposition of the lowermost part of the *Whiteinella archaeocretacea* Zone (UC3 to UC4 zones), where nannofossil-derived fertility indices reach high values and the small *Zeugrhabdotus* gr. predominates over *Biscutum* spp. The temperature index based on calcareous nannofossil assemblages indicates a warming at the beginning of the OAE2, followed by progressive cooling (the same trend indicated by $\delta^{18}O_{bulk}$ values). The significant proportion of holococcoliths suggests high-stress conditions in surface waters during most of the OAE2 interval. The enrichment in redox-sensitive elements, together with the abundance of low-oxygen tolerant benthic foraminifera, indicates dysoxic conditions both in the deep-water column and sea-bottom at the beginning of the OAE2 (*W. archaeocretacea* Zone). Geochemical detrital proxies indicate an enhanced rate of terrigenous supply during the OAE2 interval resulting from increased riverine influx related to a more humid climate. Enhanced fluvial run-off increased nutrient input to marine surface waters contributing to eutrophication (recorded by calcareous nannoplankton and planktic foraminifera). Plankton consumption of surface water nutrients increased organic matter production, whose decay contributed to the decrease in dissolved oxygen, generating increasingly dysoxic/anoxic conditions and favoring preservation of organic matter. Although low-latitude nannofossil assemblages such as those of Oued Bahloul reflect an increase in nutrient availability during the OAE2 interval, assemblages from mid-latitude areas record a decreased nutrient content.

1. Introduction

The latest Cenomanian–earliest Turonian time interval was marked by palaeoclimatic and palaeoceanographic perturbations, associated with long-lasting carbon isotope anomalies related to an oceanic anoxic event (OAE2; Huber et al., 2002; Monteiro et al., 2012; Erba et al., 2013). Two main hypotheses have been proposed to explain deposition of organic-rich facies: a) oceanic anoxia prevented the decaying of organic matter by decreased oxygen supply to the deep ocean due to slowed oceanic circulation (e.g., Erbacher et al., 2001; Tsandev and Slomp, 2009), and b) enhanced surface water productivity either from intensified upwelling or from increased weathering and run-off and water-column oxygen depletion through the decay of organic matter (e.g., Sarmiento et al., 1988; Handoh and Lenton, 2003).

The high number of calcareous nannofossil biohorizons characterizing the Upper Cenomanian-lowermost Turonian offers the opportunity to biostratigraphically constrain the OAE2. The nature of primary producers and changes of temperature in ocean surface waters during the OAE2 would need to be elucidated in order to better understand oceanic anoxic events. Calcareous nannoplankton, as a relevant group of primary producers, is ideal to address these questions because it is strongly affected by temperature, nutrient availability, pCO_2 and salinity.

The Oued Bahloul section is a classic Cenomanian–Turonian boundary locality for which previous studies focused on analysis of carbon isotopes (Amédro et al., 2005; Caron et al., 2006), sequence stratigraphy (Robaszynski et al., 1993; Accarie et al., 2000; Zagrarni et al., 2008); planktic foraminifera (Caron et al., 1999, 2006; Reolid et al., 2015) and organic geochemistry (Farrimond et al., 1990).

The only previous data on nannofossil assemblages from the Oued Bahloul section come from a stratigraphically-focused study which

* Corresponding author.
E-mail address: raguado@ujaen.es (R. Aguado).

http://dx.doi.org/10.1016/j.palaeo.2016.07.016
0031-0182/

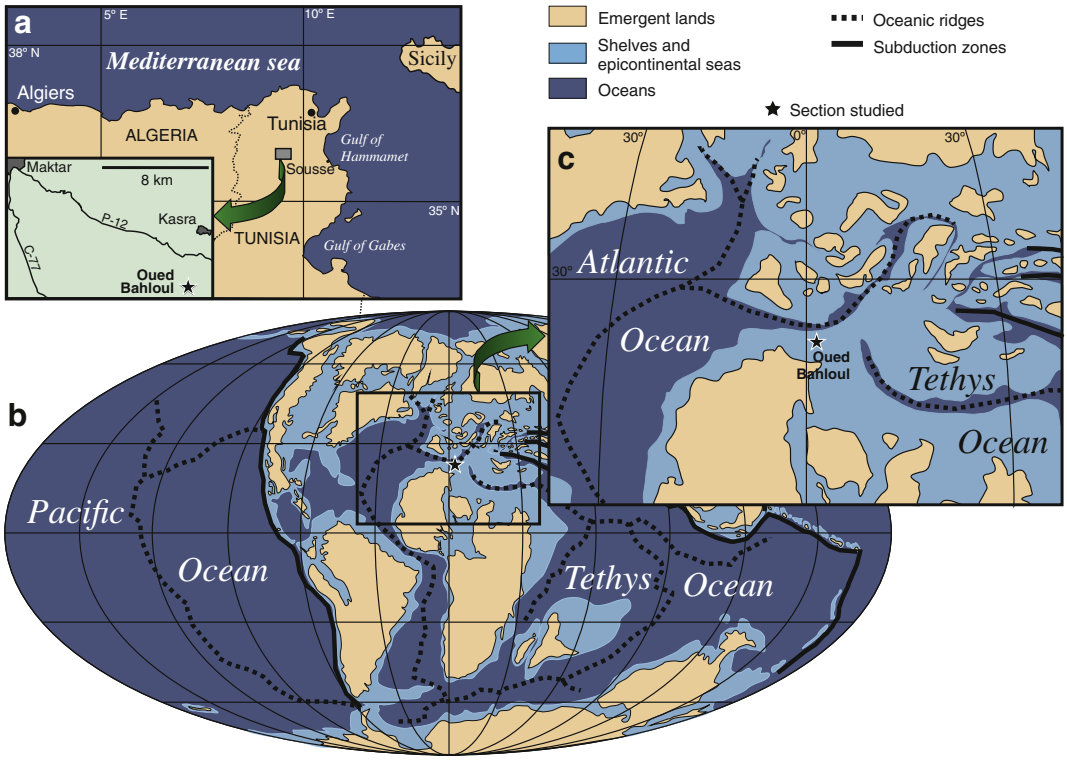

Fig. 1. A, Current geographic location of the Oued Bahloul section in central northern Tunisia. B, Global Mollweide palaeogeographic map showing the distribution of oceans and lands at the beginning of Late Cretaceous (~90 Ma) after Blakey (2005). C, A focus on the Western Tethys and North Atlantic, showing the position of the Oued Bahloul section in the Central Tunisian Platform.

included about 13 samples from this locality, containing poorly preserved assemblages (Bralower, 1988).

The aims of this research are: 1) to build a precise nannofossil biostratigraphy and make correlations with available biostratigraphic schemes based on ammonoids (Caron et al., 1999, 2006; Accarie et al., 2000; Amédro et al., 2005; Zagrarni et al., 2008) and planktic foraminifera (Caron et al., 1999, 2006; Reolid et al., 2015); 2) to carry out a quantitative and statistical analysis of the nannofossil assemblages for the reconstruction of palaeoecological and palaeoceanographic conditions during the OAE2; 3) to compare the nannofossil results with geochemical detrital, redox and productivity proxies and with foraminiferal assemblages.

2. Geological setting

The Oued Bahloul section (Fig. 1A) is located in central Tunisia, about 5 km SSW of the village of Kasra (coordinates 35° 46′ 18″ N, 9° 21′ 4″ E). At the beginning of the Late Cretaceous this section was located within the Central Tunisian Platform, at a palaeolatitude of about 15–20° N (Fig. 1B, C). During the Cenomanian–Turonian interval, central Tunisia was located in the North African continental margin (Fig. 1B) and was occupied by outer shelf facies rich in planktic foraminifera (Caron et al., 2006; Zagrarni et al., 2008; Reolid et al., 2015) where several small islands emerged which acted locally as sources of siliciclastics (Zagrarni et al., 2008).

The Oued Bahloul section is well exposed on the north-western flank of the Oued Bahloul anticline, the core of which is occupied by Cenomanian marls of the Fahdène Formation. The interval studied (47 m thick) includes the uppermost 5 m of the Fahdène Formation, the Bahloul Formation (29 m thick) and the lowermost 13 m of the Kef Formation (Fig. 2). The uppermost part of the Fahdène Formation consists of an alternation of grey-greenish marls and light-colored limestones. The overlying Bahloul Formation is divided into two members: the lower Pre-Bahloul Member and the upper Bahloul *s. str.* Member (Fig. 2). The Pre-Bahloul Member is 3.4 m thick. Its basal bed (0.5 m thick) consists of a microconglomeratic sandy limestone body that contains quartz and phosphatic black pebbles which are normally graded. The base of this body is irregular and incises the underlying marls of the Fahdène Formation. The overlying level is a bioclastic-rich calcarenite, while the uppermost part of this member consists of marls. The abrupt vertical change from the Fahdène Formation to the Pre-Bahloul Member suggests a clear discontinuity interpreted by Robaszynski et al. (1990, 1993) as a sequence boundary (Ce SB5 sensu Hardenbol et al., 1998). The whole Pre-Bahloul Member has been interpreted as a shelf margin wedge (Zagrarni et al., 2008).

Above the Pre-Bahloul Member the lithology is replaced abruptly by laminated black limestone layers (2–5 cm thick) and grey marls rich in organic matter that are characteristic of the Bahloul *s. str.* Member (hereinafter Bahloul Member). The black limestone layers are organized in couplets about 50 cm thick, which alternate with grey marls

Fig. 2. Lithological sketch of the Oued Bahloul section showing the main calcareous nannofossil bioevents found in this study and biozones according to Sissingh (1977), Perch-Nielsen (1985) and Burnett (1998). Sequence stratigraphy after Robaszynski et al. (1990, 1993). Ammonite biostratigraphy after Caron et al. (1999, 2006), Accarie et al. (2000), Amédro et al. (2005) and Zagrarni et al. (2008). Planktic foraminiferal biostratigraphy after Caron et al. (2006) and Reolid et al. (2015). Carbonate, TOC and $\delta^{18}O_{bulk}$ and $\delta^{13}C_{bulk}$ curves after Reolid et al. (2015). Extra $\delta^{13}C_{bulk}$ and $\delta^{18}O_{bulk}$ data after Amédro et al. (2005), Caron et al. (2006) (diamonds) and Zagrarni et al. (2008) (triangles). Fluctuations of the calcareous nannofossil species richness, absolute abundance (nannofossils/g of sediment), preservation (squares) and diversity indices (Shannon-H: circles, Dominance: squares, and Fisher-α: circles) throughout the section. Preservation classes: P = poor, PM = poor to moderate, MP = moderate to poor, M = moderate, MG = moderate to good, and GM = good to moderate. Shaded horizontal band corresponds to poorly preserved assemblages (see text for details).

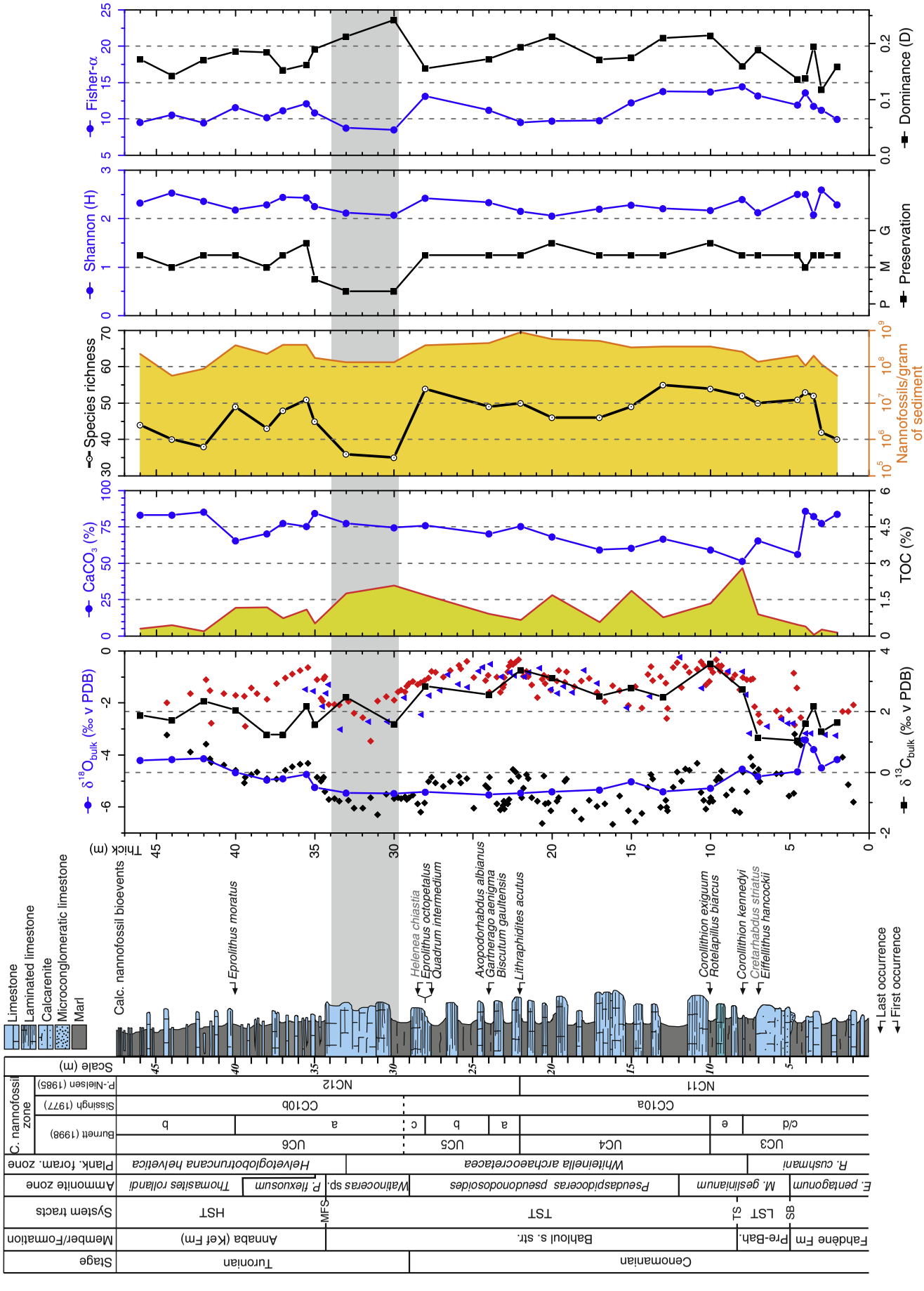
Stage
Cenomanian
Turonian
Member/Formation
Fahdène Fm
Pre-Bah.
Bahloul s. str.
Annaba (Kef Fm)
System tracts
LST
TST
HST
SB
TS
MFS
Ammonite zone
E. pentagonum
M. geslinianum
Pseudaspidoceras pseudonodosoides
Watinoceras sp.
P. flexuosum
Thomasites rollandi
Plank. foram. zone
R. cushmani
Whiteinella archaeocretacea
Helvetoglobotruncana helvetica
C. nannofossil zone
Burnett (1998)
Sissingh (1977)
P.-Nielsen (1985)
UC3
UC4
UC5
UC6
c/d
e
a
b
c
CC10a
CC10b
NC11
NC12
Scale (m)
Limestone
Laminated limestone
Calcarenite
Microconglomeratic limestone
Marl
Calc. nannofossil bioevents
Eprolithus moratus
Helenea chiastia
Eprolithus octopetalus
Quadrum intermedium
Axopodorhabdus albianus
Gartnerago aenigma
Biscutum gaultensis
Lithraphidites acutus
Corollithion exiguum
Rotelapillus biarcus
Corollithion kennedyi
Cretarhabdus striatus
Eiffellithus hancockii
Last occurrence
First occurrence
Thick (m)
δ18Obulk (‰ v PDB)
CaCO3 (%)
Species richness
Nannofossils/gram of sediment
TOC (%)
δ13Cbulk (‰ v PDB)
Fisher-α
Shannon (H)
Dominance (D)
P
M
G
Preservation

throughout this member (25.6 m width), although rhythmicity tends to fade towards the top of the interval. In detail, the black limestones are composed of dark-colored laminae rich in organic matter containing radiolaria, benthic and planktic foraminifera, and light-colored laminae that contain mostly planktic foraminifera (Caron et al., 2006). The grey marls are bioturbated and lamination is not observed. The transition from black limestones to grey marls is gradual, while the transition from grey marls to black limestones is abrupt. The top of the Bahloul Member consists of a centimetric highly-bioturbated bed, rich in ammonite moulds and containing phosphate and glauconite grains, which is included within limestones rich in filaments (filament event). In terms of sequence stratigraphy, lithologic change between the Pre-Bahloul Member and Bahloul Member has been interpreted as a transgressive surface (Ce TS5 of Hardenbol et al., 1998), the deepening upwards cycles of the Bahloul Member as a transgressive systems tract, and the top of the Bahloul Member as the maximum flooding surface (Fig. 2; Robaszynski et al., 1990, 1993; Zagrarni et al., 2008).

The overlaying Annaba Member of the Kef Formation consists of marl–limestone alternations displaying shallowing upward cycles, and is interpreted as a highstand systems tract (Zagrarni et al., 2008).

3. Materials and methods

3.1. Sample treatment

Fractions of the same samples used in Reolid et al. (2015) were used for calcareous nannofossil investigation. In total 25 unevenly spaced samples were collected throughout the studied interval. Smear slides of all collected samples were prepared following the decantation method described in Geisen et al. (1999) and examined using a polarizing light microscope Olympus BHSP at 1200× magnification. Potential carbonate dissolution was checked by examination of simple smear slides of unprocessed sample material. At least 450 determinable nannofossil specimens (average 756) were counted on each slide in order to perform an analysis of the assemblage composition. In addition, smear-slide investigation was extended to complete a minimum of 400 fields of view (1 field of view = 2.37×10^{-2} mm^2) along a longitudinal traverse in order to report the presence of rare taxa. The taxonomic framework used (Figs. 3–4 and Appendix A, B) is based on Perch-Nielsen (1985), Bown et al. (1998), Kennedy et al. (2000), Lees (2007), and Aguado (2012). All calcareous nannofossils with more than half of the specimens preserved were included in the counts.

Nannofossil preservation for individual samples was evaluated directly from the observation of smear slides in the polarizing microscope using the visual criteria introduced by Roth and Thierstein (1972). In addition, percentage abundances of some diagenesis-resistant taxa, especially *Watznaueria* (see Section 4.1) were also used to evaluate the preservation of assemblages in individual samples (Fig. 5).

3.2. Diversity, statistical and palaeoecological analyses

Simple diversity (species richness) was calculated for each sample. In addition, the Shannon–Wiener Index H (Shannon and Weaver, 1949); Dominance (Simpson, 1960) and Fisher-α diversity (Fisher et al., 1943), as implemented in the PAST software v3.11 (Hammer et al., 2001), were calculated from species census counts in order to further evaluate ecological signals in the assemblages (Fig. 2).

The absolute (nannofossils per gram of rock; Geisen et al., 1999) and relative (% of single taxa relative to total assemblage) abundances were calculated from species census counts. For the quantitative analyses of the assemblages, some taxa were grouped at a generic level, such as *Biscutum* spp. (*B. constans*: Fig. 3ab–ad, and *B. gaultensis*: Fig. 3ae–ag), *Eiffellithus* spp. (Fig. 3cp–cs), *Prediscosphaera* spp., *Retecapsa* spp., and *Watznaueria* spp. Other groupings include the small *Zeugrhabdotus* gr. (*Z. erectus*: Fig. 3o, *Z. howei*: Fig. 3p–v, and *Z. noeliae*: Fig. 3w–aa) and *Eprolithus* gr. (*E. floralis*: Fig. 4g–i, *E. moratus*: Fig. 4s, *E. octopetalus*: Fig. 4j, r, and the related *Radiolithus planus*: Fig. 4k–m). The holococcoliths (*Bilapillus wadeae*: Fig. 3bn–bz, *Calculites percernis*: Fig. 3cn, co, *Orastrum perspicuum*: Fig. 3cl, cm, *Owenia hillii*: Fig. 3cb–ck, and *O. dispar*: Fig. 3ca) were also grouped together as they represent haptophyte haploid stages that probably developed in response to environmental stress (Section 5.3; Mutterlose and Bottini, 2013). After these groupings, only those taxa having a mean relative abundance higher than 1% were selected as significant for statistical analysis (Figs. 6, 7). However, the rare taxa *Discorhabdus ignotus* (Fig. 3as–av, average 0.72%) and *Rhagodiscus asper* gr. (*R. asper*: Fig. 4a–c, and *R. splendens*: Fig. 4d–f; average 0.16%) were also considered because of their presumed palaeoecological significance (Roth and Krumbach, 1986; Mutterlose, 1987; Bottini and Mutterlose, 2012; Aguado et al., 2014a, b). The taxa included in the selected groups account for 87.8% to 95.1% (average 91.9%) of the individuals in the assemblages. The rest of the taxa were all considered together within the 'other taxa' group (Fig. 7).

In order to better constrain the statistical significance of peaks in nannofossil abundances, confidence intervals for percentages were calculated (Figs. 6, 7) using approaches proposed for multinomial proportions (Heslop et al., 2011). For an error rate $\alpha = 0.05$, these limits define the 95% confidence intervals associated with the percentage of each taxon in a sample (Pagano, 2013). Calculations were made using the statistical software available at https://www.marum.de/Software_and_Programs.html#Section19526.

The relative abundances (percentages) of taxa with special palaeoecological significance were used in the calculation of productivity index (PI; Gale et al., 2000), nannoplankton index of productivity (NIP; Eshet and Almogi-Labin, 1996), and temperature index (TI; Bornemann et al., 2005), which were selected due to its better adaptation to the composition of the studied assemblages. These indices were implemented as follows:

$$\mathrm{PI} = (\%\textit{Biscutum}\ \text{spp.} + \%\text{small Zeugrhabdotus spp.})/\%\textit{Watznaueria}\ \text{spp.} \quad (1)$$

$$\mathrm{NIP} = \mathrm{Log}_{10}\ [(\%\textit{Biscutum}\ \text{spp.} + \%\textit{Zeugrhabdotus}\ \text{spp.}) / (\%\textit{Eiffellithus}\ \text{spp.} + \%\textit{Lithraphidites}\ \text{spp.} + \%\textit{M.decoratus} + \%\textit{Prediscosphaera}\ \text{spp.} + \%\textit{Staurolithites}\ \text{spp.})] \quad (2)$$

$$\mathrm{TI} = \%\textit{T.orionatus}/\%\textit{Rhagodiscus}\ \text{spp.} \quad (3)$$

Low values of PI from 0 to 0.5 characterize low nutrient availability, whereas values above 1 are typical for high nutrient availability and thus higher productivity (see also Linnert et al., 2010; Pavlishina and Wagreich, 2012). NIP values around and above zero characterize high-productivity settings, whereas values around −2 characterize low-productivity settings (Eshet and Almogi-Labin, 1996; Pavlishina and Wagreich, 2012).

3.3. Elemental analyses

Whole-rock analyses of major elements were carried out on all sampling levels using X-ray fluorescence (XRF; Philips PW 1040/10 spectrometer). The content of trace elements was determined using an inductively coupled plasma-mass spectrometer (ICP-MS Perkin Elmer Sciex-Elan 5000) at the Centro de Instrumentación Científica (Universidad de Granada). The instrumental error was ±2% and ±5% for elemental concentrations of 50 ppm and 5 ppm, respectively.

Some of these geochemical data were used by Reolid et al. (2015) to estimate palaeoproductivity (Sr/Al, U/Al and P/Ti ratios) and redox conditions (Co/Al, Cu/Al, Cr/Al, Ni/Al, Th/Al ratios and enrichment factors and authigenic values of Mo and U). These geochemical proxies are compared with calcareous nannofossil assemblages. Moreover, distinct major and trace elements/Al ratios were selected for interpreting fluvial transport (K/Al; Chester et al., 1977) and aeolian transport (Zr/Al and Ti/Al; Pye, 1987; Reolid et al., 2012) in the detrital input. In addition, the elemental ratio D* (Machhour et al., 1994) expressed as Al / (Al + Fe + Mn) was used as a general detrital proxy.

4. Results

4.1. Calcareous nannofossil preservation

Average preservation of calcareous nannofossil assemblages in the study section, from visual estimation, is moderate to good (Fig. 2). However, two of the samples (OB-30 and OB-33 m) are characterized by poorly preserved assemblages. Absolute abundance drops for these samples and diversity parameters as species richness, Shannon H and Fisher-α also show a decrease (Section 4.2), while the dominance parameter increases and reaches its maximum values, mainly due to the increase in abundance of dissolution-susceptible taxa such as *Biscutum* spp., or small *Zeugrhabdotus* gr. (Thierstein, 1980). In addition, the increase in relative abundance of the dissolution-resistant *Watznaueria* spp. (Roth and Bowdler, 1981; Roth and Krumbach, 1986) in samples OB-30 and OB-33 m does not correlate with an increase in its absolute abundance (Fig. 6). This suggests that this increase in relative abundance of *Watznaueria* spp. is an artifact consequence of the closed sum effect induced by poor preservation.

High proportions of *Watznaueria* spp. in poorly preserved calcareous nannofossil assemblages correlate inversely with total abundance and diversity. The correlation coefficients of percentage abundances of this taxon with respect to both simple diversity and total nannofossil abundances are low for the studied interval (Fig. 5a, b). However, we can see that samples OB-30 and OB-33 m are the only outliers due to their higher percentage abundance in *Watznaueria* spp. The degree of correlation between bulk rock carbon and oxygen isotopes ($\delta^{13}C_{bulk}$ and $\delta^{18}O_{bulk}$), which has been used (Corfield, 1995; Duchamp-Alphonse et al., 2007; Aguado et al., 2008) as an indicator of the extent of diagenetic alteration in carbonate rocks, is low throughout Oued Bahloul section (Fig. 5c).

All the above indicates that the calcareous nannofossil assemblages of the study material were not significantly altered by diagenetic processes and, with the exception of those from samples OB-30 and OB-33 m, they represent the original biocenosis and preserve palaeoenvironmental signals.

4.2. Diversity of calcareous nannofossil assemblages

A total of 89 taxa (Appendix B) were identified in the studied interval, where all samples examined contained calcareous nannofossils. Average species richness is higher throughout the lower part (Cenomanian) than throughout the upper (Turonian) part of the section (Fig. 2). A drastic drop in species richness (~36 taxa) is found in the uppermost part of the Bahloul Member (samples OB-30 and OB-33 m, just below the *Helvetoglobotruncana helvetica* Zone). The curve of Fisher-α diversity is consistent with that of the species richness (Fig. 2).

No great fluctuations of Shannon Index are recorded throughout the studied interval, with the exception of a drop at the top (samples OB-30 and OB-33 m) of the Bahloul Member (Fig. 2). This drop is a consequence of poorer preservation (Section 4.1) which, in turn, results in a decrease in absolute abundance of calcareous nannofossils and an increase in relative (but not in absolute) abundance of *Watznaueria* spp. (Fig. 6). This drop is related to the increase in the dominance that is recorded for the same levels and is the most prominent feature of the Dominance (D) curve (Fig. 2). There is no apparent correlation between diversity indices and carbonate content or TOC values.

4.3. Biostratigraphy

The 13 calcareous nannofossil bioevents identified (Fig. 2) allowed the application of multiple zonations to the studied section. The zones CC10a and CC10b of Sissingh (1977), NC11 and NC12 of Perch-Nielsen (1985), and UC3 (subzones c/d and e), UC4, UC5 (subzones a, b, and c) and UC6 (subzones a and b) of Burnett (1998) were identified. The last occurrence (LO) of *Lithraphidites acutus* (Fig. 4n–p) in sample OB-22 m was used to place the limit between the NC11 and NC12 zones, according to the zonation of Perch-Nielsen (1985). The boundary between CC10a and CC10b zones of Sissingh (1977) has to be placed coinciding with the LO of *Helenea chiastia* (Fig. 3cy–cz). As a consequence of the sampling interval, this bioevent was recorded in sample OB-28 m together with the first occurrences (FOs) of *Eprolithus octopetalus* (Fig. 4j, r) and *Quadrum intermedium* (Fig. 4t). However, it is known (e.g., Burnett, 1998; Tantawy, 2008) that the LO of *H. chiastia* is younger than the FOs of *E. octopetalus* and *Q. intermedium*. As *H. chiastia* was not found in sample OB-30 m, the boundary between CC10a and CC10b zones was tentatively placed slightly above 29 m (Fig. 2), about 40 cm over the FO of *Watinoceras* sp. (see Burnett, 1998). Isolated and poorly preserved specimens of *H. chiastia* were found in samples at 38 and 40 m, within the Annaba Member (Kef Formation), but were considered as reworked.

The LO of *Corollithion kennedyi* (Fig. 3bb–bf) in sample OB-8 m was used to place the boundary between UC3d and UC3e subzones according to Burnett (1998). The stratigraphic interval below sample OB-8 m has to be assigned to the subzones UC3c/d undifferentiated due to the presence of *Lithraphidites acutus* and the absence of *Staurolithites gausorhethium* and *Gartnerago nanum*. The FO of *Rotelapillus biarcus* (Fig. 3bg–bm) in sample OB-10 m was used to place the boundary between zones UC3 and UC4. Subzones UC4a and UC4b could not be differentiated in Oued Bahloul because of the presence of the last record of *Cretarhabdus striatus* (Fig. 3da) in sample OB-7 m. The LO of *Axopodorhabdus albianus* (Fig. 3ct–cx) in sample OB-24 m marks the boundary between subzones UC5a and UC5b. The lower limit of the subzone UC5c was placed in sample OB-28 m, coinciding with the FO of *Quadrum intermedium*. The boundary between zones UC5 and UC6 is marked by the LO of *H. chiastia*. This boundary was tentatively placed slightly above OB-29 m. Finally, the FO of *Eprolithus moratus* (Fig. 4s) at sample OB-40 m allowed the identification of UC6a and UC6b subzones.

Some other FOs and LOs were identified in addition to the bioevents used as index species in the applied zonations. The LO of *Eiffellithus hancockii* (Fig. 3cp) was recorded in sample OB-7 m and the FO of *Corollithion exiguum* (Fig. 3aw–ba) in sample OB-10 m. These are followed by the LOs of *Gartnerago aenigma* (Fig. 3a–f) and *Biscutum gaultensis* (Fig. 3ae–ag) in sample OB-24 m and the FO of *Eprolithus octopetalus* in sample OB-28 m. The FO of *Quadrum gartneri* was not observed in the studied interval of Oued Bahloul section. The vertical distribution of biostratigraphic index taxa and major bioevents together with the zones identified is summarized in Fig. 2. In this figure, the nannofossil zones are correlated with respect to planktic foraminifera (Caron et al., 2006; Reolid et al., 2015) and ammonite (Caron et al., 1999, 2006; Accarie et al., 2000; Amédro et al., 2005) biostratigraphies.

4.4. Absolute and relative abundances

The average absolute abundance is clearly higher throughout the Bahloul Formation than in the Fahdène and the Kef formations (Fig. 2). Fluctuations in absolute abundance throughout the section do not seem to be linked to calcium carbonate or TOC content (Fig. 2).

With average absolute abundance of 8.70 × 10^7 n/g, the small *Zeugrhabdotus* gr. constitutes the most common taxon in Oued Bahloul section. The mean absolute abundances of other common taxa are *Biscutum* spp.: 5.41 × 10^7, *Watznaueria* spp.: 4.86 × 10^7, *Eiffellithus* spp.: 1.82 × 10^7, and *Prediscosphaera* spp.: 1.60 × 10^7 n/g. The absolute abundances of most common taxa are represented in Figs. 6 and 7.

Only three of the most common taxa, small *Zeugrhabdotus* gr. (29.0%), *Watznaueria* spp., (18.3%) and *Biscutum* spp., (17.4%) exceed

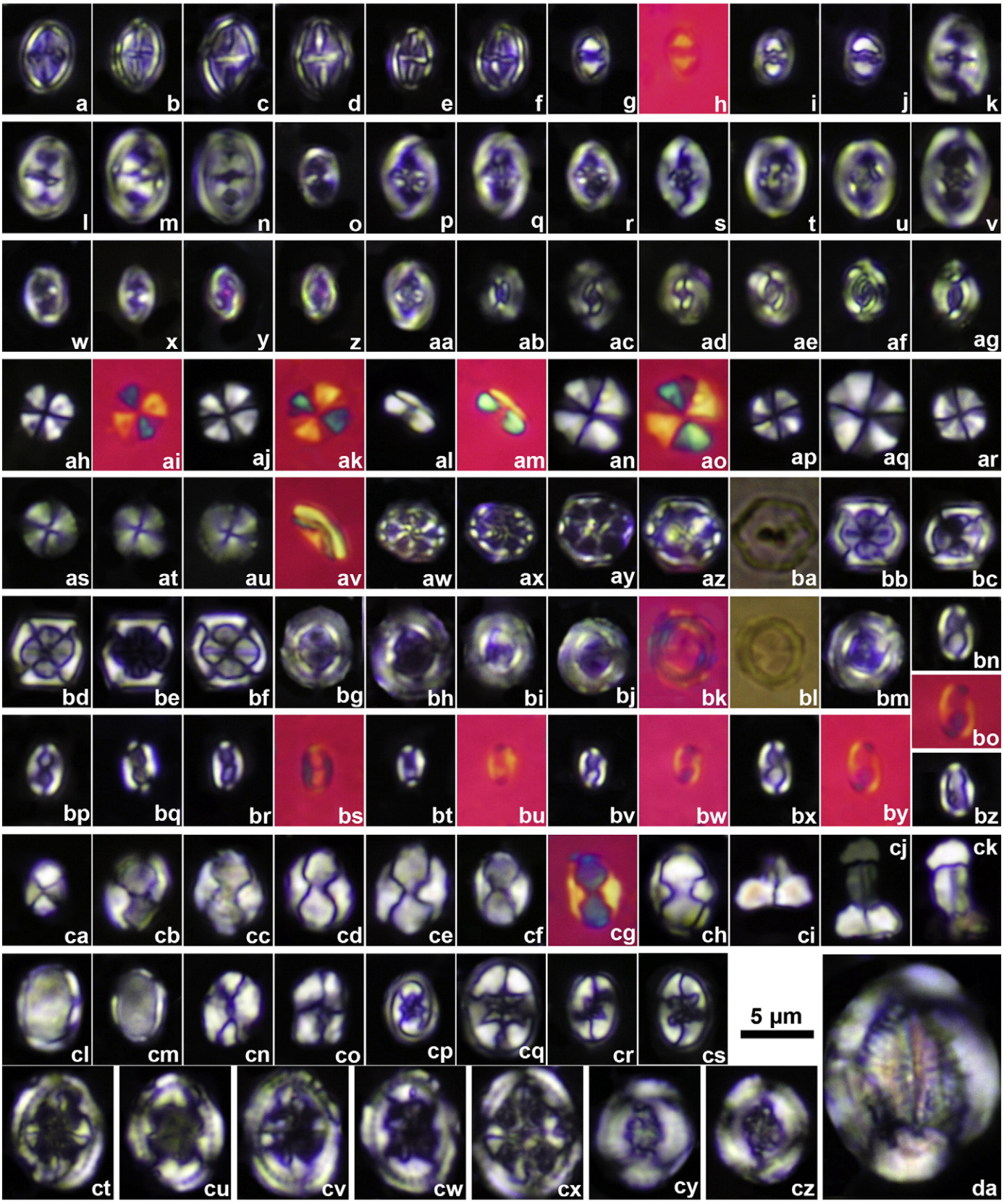

10% of average percentage abundance in the assemblages. Two taxa, *Eiffellithus* spp. (5.77%) and *Prediscosphaera* spp. (5.61%), have mean abundances greater than 5%. The species *Discorhabdus hannibalis* (Fig. 3ah–ar, 3.48%) and *Retecapsa* spp. (2.89%) have average abundances greater than 2%. The additional taxa used in palaeoecological analyses (*Tranolithus minimus*: Fig. 3g–j, 1.84%; *Eprolithus* gr.: 1.82%; *Lithraphidites carniolensis*: Fig. 4q, 1.82%; holococcoliths = 1.39%, and *Tranolithus orionatus*: Fig. 3k–n, 1.33%; Figs. 6, 7) have mean abundances greater than 1% with the exception of *Discorhabdus ignotus* (average 0.72%) and *Rhagodiscus asper* gr. (average 0.16%) which were also considered because of their presumed palaeoecological significance. Figs. 6 and 7 summarize the results showing the fluctuations in relative abundance of these taxa.

5. Discussion

5.1. Calcareous nannofossils and palaeofertility

The OAE2 has been suggested as an episode with high surface productivity (Sarmiento et al., 1988; Farrimond et al., 1990; Handoh and Lenton, 2003; Reolid et al., 2015, 2016). Analyses of biomarkers carried out by Farrimond et al. (1990) reported abundant algal-derived organic matter across the Cenomanian–Turonian transition at Oued Bahloul, indicating high surface productivity. Calcareous nannoplankton, as part of marine phytoplankton, are affected by changes in fertility of surface waters (Rost and Riebesell, 2004), and calcareous nannofossil assemblages are a useful tool to assess palaeoproductivity and fertilization (Roth and Bowdler, 1981; Roth and Krumbach, 1986; Herrle, 2003; Kessels et al., 2003; Aguado et al., 2008, 2014a, b).

The most prominent feature of calcareous nannofossil assemblages from the Oued Bahloul section is the high abundance of the small *Zeugrhabdotus* gr. and *Biscutum* spp. throughout most of the OAE2-interval (*W. archaeocretacea* Zone, Fig. 6). In contrast, the abundance of *Watznaueria* spp. is low with the exception of two poorly preserved samples (OB-30 and OB-33 m), that were excluded from palaeoenvironmental analysis (see Sections 4.1 and 4.2). The small *Zeugrhabdotus* gr. and *Biscutum* spp. are seen as moderate to high-fertility indicators, and are more abundant in meso-eutrophic surface waters (Roth and Bowdler, 1981; Herrle, 2003; Lees et al., 2005; Bottini and Mutterlose, 2012; Aguado et al., 2014a,b). Assemblages rich in small *Zeugrhabdotus* gr. and *Biscutum* spp. are typical for continental margins with intense upwelling of nutrient-rich waters (Roth and Bowdler, 1981) or shallow epicontinental seas with high continental nutrient run-off and/or storm mixing (Street and Bown, 2000; Herrle, 2003; Kessels et al., 2003). The maximum values of these taxa in Oued Bahloul (Fig. 6) suggest that eutrophic surface waters developed during deposition of the uppermost part of Fahdène Formation, lower part of Pre-Bahloul Member, and most of the lower and middle part of Bahloul Member (Fig. 6).

Owing to its inverse correlation with percentages of meso-eutrophic taxa, *Watznaueria* spp. is usually associated with oligotrophic surface waters linked to low-productivity settings (Roth and Krumbach, 1986; Herrle, 2003; Bottini and Mutterlose, 2012). However, this negative correlation may, in some instances, be the result of a closed sum artifact (Lees et al., 2005). This is the case for samples OB-30 and OB-33 m, where the percentages of *Watznaueria* spp. increase simply because those of other abundant taxa (small *Zeugrhabdotus* gr. and especially *Biscutum* spp.) decrease. *Watznaueria* spp. is here regarded as a robust eurytopic taxon, able to adapt to fluctuating environmental conditions more efficiently than some other species (Mutterlose, 1991; Street and Bown, 2000; Aguado et al., 2014b). As a result, the percentage abundance of *Watznaueria* spp. may be used as a measure of the success of other species rather than as a direct response to an environmental signal.

In order to quantify surface water fertility throughout Oued Bahloul section, the PI (Gale et al., 2000) and NIP (Eshet and Almogi-Labin, 1996) were selected due to better adaption to the composition of nannofossil assemblages, and calculated for each sample (Section 3.2). Fig. 9 summarizes the fluctuations of PI and NIP throughout the study section. Both indices display high values (see Section 3.2) throughout the studied interval, indicating generalized meso-eutrophic surface waters. As each index relies on different taxa, they display some differences but there are also intervals (marked and numbered 1 to 4 in Fig. 8) in which they show agreement, both taking especially high values. The first short interval with high values of the PI and NIP (1 in Fig. 8) is located immediately below the main excursion in $\delta^{13}C_{bulk}$ curve, indicating the onset of the OAE2 interval. It correlates with a short excursion of the $\delta^{13}C_{bulk}$ values recorded near the top of the Fahdène Formation and is interpreted as a short pulse predating the more extreme palaeoenvironmental conditions developed during the OAE2. This short pulse may be related to the pulse in P mobilization and burial described by Mort et al. (2007a) at the onset of OAE2. However, the most prominent maxima indicating high productivity of surface waters, especially as displayed by PI, are those within the Bahloul Member. The first one (2 in Fig. 8) is located near the base of the Bahloul Member (around UC3 and UC4 zones boundary), while the second one (3 in Fig. 8) falls around its middle part (close to UC4 and UC5 zones boundary). Finally, a new short interval with high values of the productivity indices (4 in Fig. 8) is recorded within the lowermost part of the Annaba Member. The distribution of maxima and minima in these indices (especially in PI) broadly agrees and correlates with the fluctuations in $\delta^{13}C_{bulk}$ curves, which provides additional support for their significance.

In detail, the peaks in the percentages of the small *Zeugrhabdotus* gr. and those of *Biscutum* spp. throughout the study section do not match

Fig. 3. Cross-polarized light micrographs of selected calcareous nannofossils from Oued Bahloul section. For each specimen, numbers in parentheses correspond to the sample, which are followed by the angle of orientation with respect to crossed nicols if applicable. Simple polarized light (P) or gypsum plate (GP) inserted (fast ray oriented NW-SE) specifically indicated. a–f, *Gartnerago aenigma* com. nov.; a, f, (OB-4), 30°; b, (OB-17), 30°; c–e, (OB-24); c, d are same specimen at 45° and 25°, e, 25°. g–j, *Tranolithus minimus*; g, h, are same specimen, (OB-37), 15°, h = GP; i, (OB-4), 0°; j, (OB-44), 10°. k–n, *Tranolithus orionatus*; k, (OB-10), 0°; l, m, (OB-20), 0°; n, (OB-44), 0°. o, *Zeugrhabdotus erectus*, (OB-4.5), 35°. p–v, *Zeugrhabdotus howei*; p, q, (OB-20), same specimen at 0° and 45°; r, (OB-24), 45°; s, (OB-4.5), 45°; t, u, (OB-46), specimen at 0° and 45°; u, (OB-44), 45°. w–aa, *Zeugrhabdotus noeliae*; w, x, (OB-20), 5° and 0°; y, z, (OB-46), same specimen at 0° and 45°; aa, (OB-4.5), 35°. ab–ad, *Biscutum constans*; ab, ac, (OB-10), 15° and 30°; ad, (OB-3.5), 25°. ae–ag, *Biscutum gaultensis*; ae, (OB-10); af, ag, (OB-7), same specimen at 35° and 40°. ah–ar, *Discorhabdus hannibalis*; ah, ai, (OB-3.5), holotype, same specimen, ai = GP; aj, ak, (OB-13), paratype, same specimen, ak = GP; al, am, (OB-3.5), paratype side view, same specimen, am = GP; an, ao, (OB-3.5), same specimen, ao = GP; ap, aq, (OB-3); ar, (OB-4). as–av., *Discorhabdus ignotus*; as, (OB-4.5); at, au, (OB-3); av., (OB-4), side view with GP. aw–ba, *Corollithion exiguum*; aw, (OB-10), ax, (OB-13), ay–ba, (OB-46), az and ba are same specimen, ba, P. bb–bf, *Corollithion kennedyi*; bb, (OB-8), 15°; bc, (OB-3.5), 15°; bd, be, (OB-4.5), same specimen at 0° and 40°; bf, (OB-8), 15°. bg–bm, *Rotelapillus biarcus*; bg, bh, (OB-13); bi, (OB-20); bj–bl, (OB-35.5), same specimen, bk = GP, bl = P; bm, (OB-40). bn–bz, *Bilapillus wadeae*; bn, bo, bz, (OB-37), same specimen, 45°, GP, and 0°; bp, (OB-22), 40°; bq, (OB-35.5), 45°; br, bs, (OB-37), same specimen 0° and GP respectively; bt–bw, (OB-37), same specimen 0°, GP, 40° and GP, respectively; bx, by, (OB-37), same specimen, 0° and 45° respectively. ca, *Owenia dispar*, (OB-44), 35°; cb–ck, *Owenia hillii*; cb, cc, (OB-10), 35° and 10° respectively; cd, (OB-20), 45°; ce, (OB-28), 30°; cf., cg, (OB-28), 40°, and GP respectively; ch, (OB-35.5), 45°; ci, (OB-30), side view 10°; cj, ck, (OB-33), side views at 15° and 45°. cl, cm, *Orastrum perspicuum*; cl, (OB-20), 35°; cm, (OB-24), 35°. cn, co, *Calculites percernis* (OB-22), same specimen at 45° and 0°. cp, *Eiffellithus hancockii*, (OB-4), 25°. cq–cs, *Eiffellithus casulus*; cq, (OB-10), 40°; cr, cs, (OB-8), 15° and 25° respectively. ct–cx, *Axopodorhabdus albianus*; ct, cu, (OB-7), same specimen at 15° and 45°; cv, cw, (OB-13), same specimen at 30° and 55°; cx, (OB-15), 15°. cy, cz, *Helenea chiastia*; cy, (OB-20), 20°; cz, (OB-4.5), 40°. da, *Cretarhabdus striatus*, (OB-4), 0°.

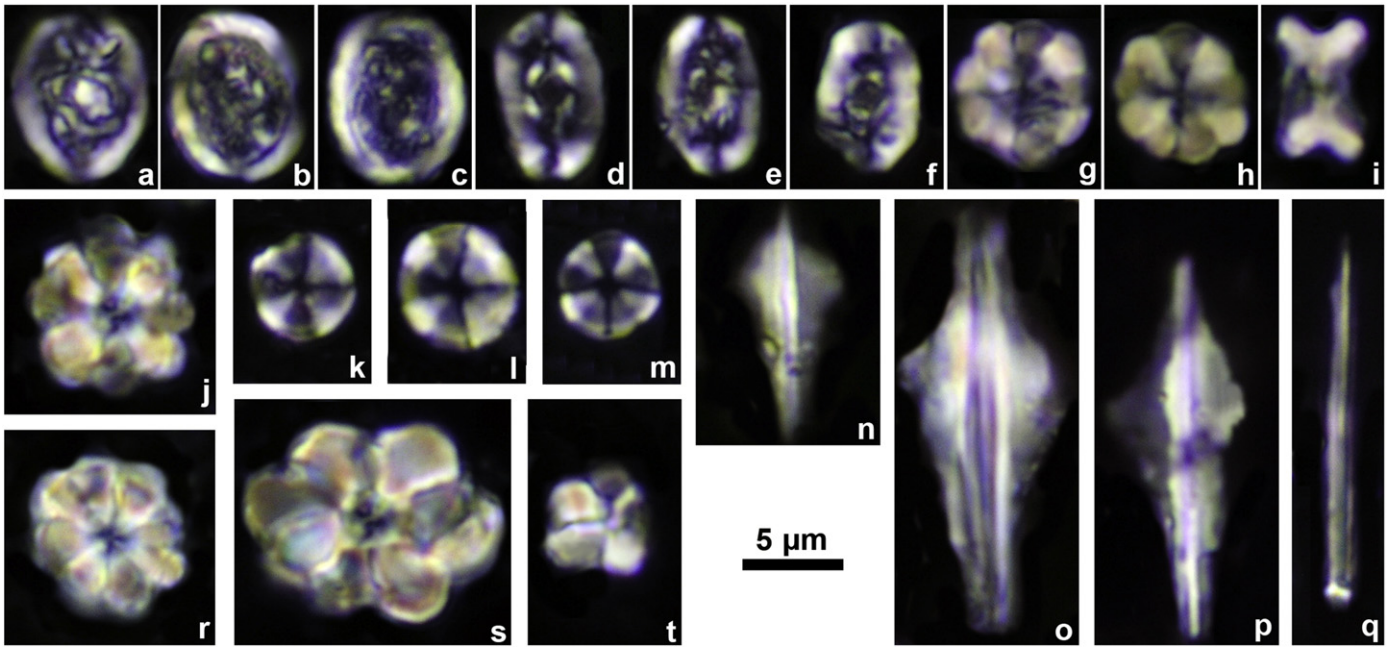

Fig. 4. Cross-polarized light micrographs of selected calcareous nannofossils from Oued Bahloul section. For each specimen, numbers in parentheses correspond to the sample, which are followed by the angle of orientation with respect to crossed nicols if applicable. a–c, *Rhagodiscus asper*; a, (OB-13), 0°; b, (OB-28), 45°; c, (OB-8), 30°. d–f, *Rhagodiscus splendens*; d, (OB-28), 30°; e, (OB-37), 30°; f, (OB-4.5), 30°. g–i, *Eprolithus floralis*; g, (OB-13); h, (OB-35.5); i, (OB-10), side view. j, r, *Eprolithus octopetalus*, (OB-38). k–m, *Radiolithus planus*; k, l, (OB-10); m, (OB-20). n–p, *Lithraphidites acutus*; n, (OB-20), 45°; o, (OB-13), 30°; p, (OB-4.5), 45°. q, *Lithraphidites carniolensis*, (OB-20), 35°. s, *Eprolithus moratus*, (OB-40). t, *Quadrum intermedium*, (OB-28).

(Figs. 6 and 8). Although both taxa are associated with elevated nutrient levels, the ecological preferences of the two species are thought to have differed slightly (Erba, 1992; Kessels et al., 2003; Lees et al., 2005). Erba (1992) suggested higher preference of nutrients of small *Zeugrhabdotus* gr. than *Biscutum* spp. On the other hand, Kessels et al. (2003) concluded that the small *Zeugrhabdotus* gr. may reflect elevated but somewhat lower fertility conditions than *Biscutum* spp. Möller and Mutterlose (2014) observed a predominance of *Z. erectus* (included here in the small *Zeugrhabdotus* gr.) over *Biscutum* spp. in more coastal environments with assumed high nutrient levels in the Hauterivian sediments of the Lower Saxony Basin. Conversely, high abundances of *Biscutum* spp. predominated over *Z. erectus* in more pelagic environments with lower nutrient supply. If this applies to what we have observed in Oued Bahloul section, it could suggest that the more eutrophic conditions, which correlate with the highest values in the $\delta^{13}C_{bulk}$ curve, probably developed throughout deposition of the lowermost part of the Bahloul Member.

Discorhabdus ignotus is usually interpreted as a moderate to high fertility indicator, and is more abundant in meso-eutrophic surface waters (Herrle, 2003; Bornemann et al., 2005; Bottini and Mutterlose, 2012; Aguado et al., 2014b). This species is rare in Oued Bahloul, (Fig. 7) and its abundance seems to decrease even further from the base of the Pre-Bahloul Member to the top of the section. A somewhat similar behavior was observed for *D. hannibalis* (Aguado, 2012), which drastically decreases in abundance throughout the end of the Fahdène Formation and Pre-Bahloul Member (Fig. 6). The abundances of both *Discorhabdus* species appear to display inverse correlation with those of *Biscutum* spp. and the small

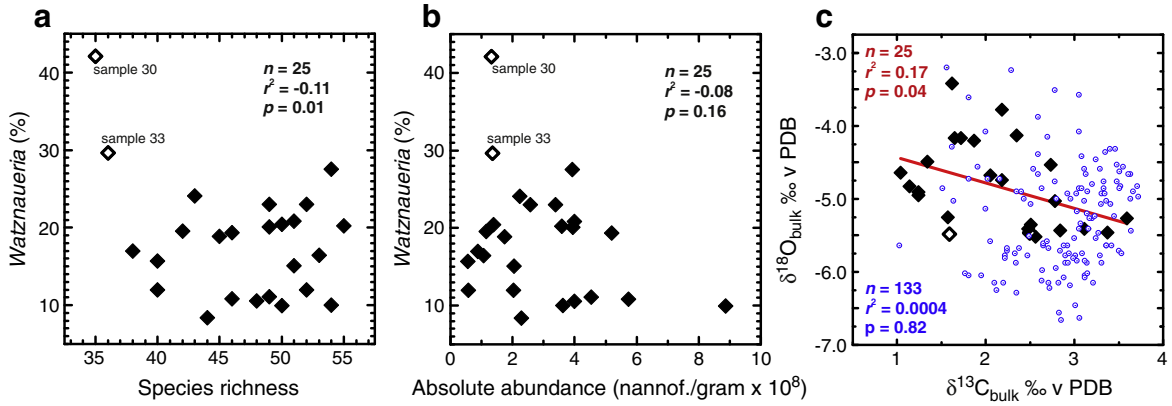

Fig. 5. Scatter plots showing the relationships between the percentages of *Watznaueria* and simple diversity (a), and percentages of *Watznaueria* and total nannofossil abundance (b). Scatter plot showing the lack of significant correlation between the $\delta^{18}O_{bulk}$ and $\delta^{13}C_{bulk}$ values (c). Black diamonds and regression line: data from Reolid et al. (2015); small circles: data from Caron et al. (2006).

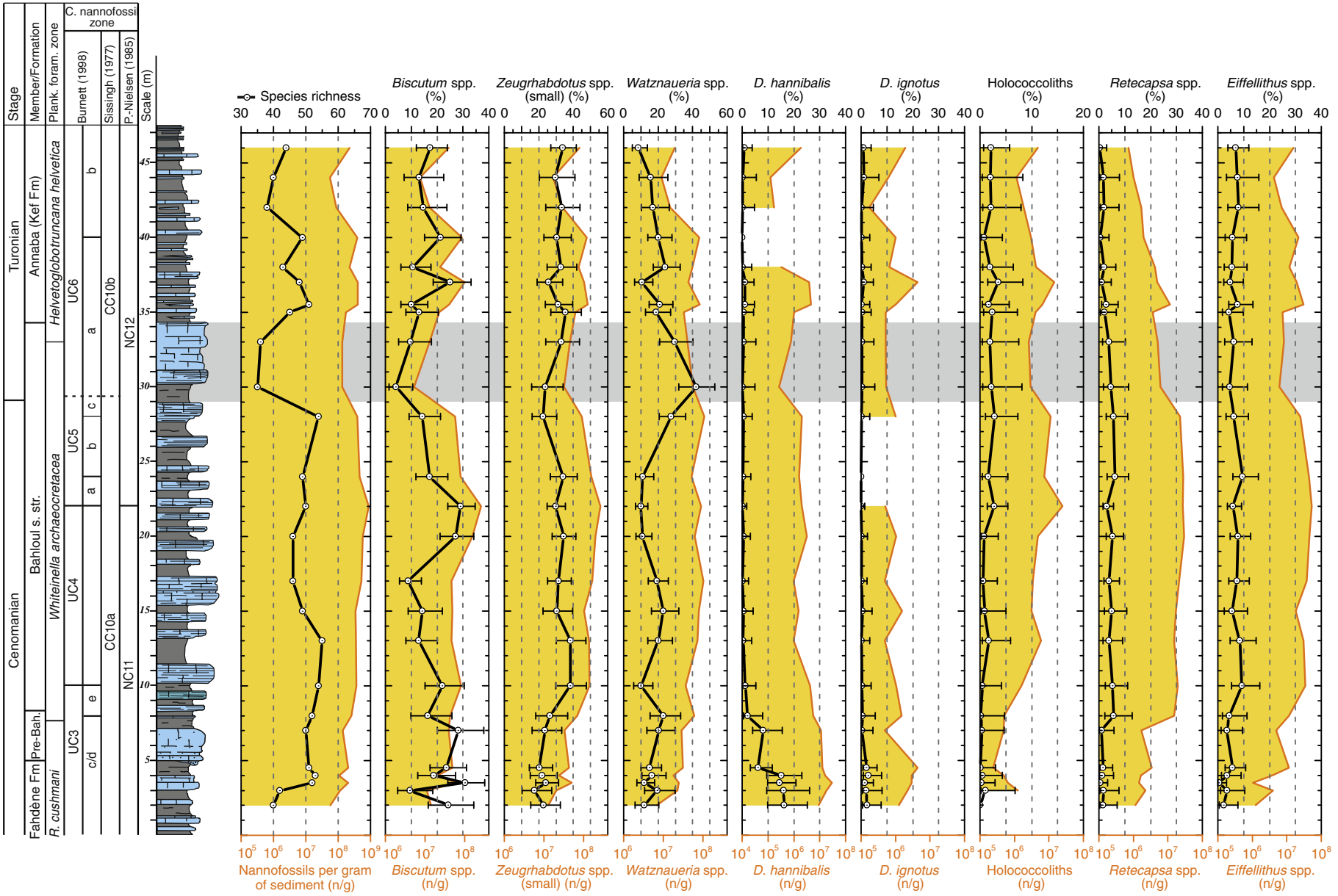

Fig. 6. Fluctuations of selected calcareous nannoplankton taxa throughout the Oued Bahloul section. Absolute abundances (individuals per gram of sediment) are represented (shaded graphs) in the bottom x-axes, while relative percentage abundances (line and error bars) are represented in the top x-axes. Lithology and biostratigraphy are as in Fig. 2. Shaded horizontal band corresponds to poorly preserved assemblages (see text for details). Breaks in *D. hannibalis* and *D. ignotus* represent intervals in which the taxa were not recorded.

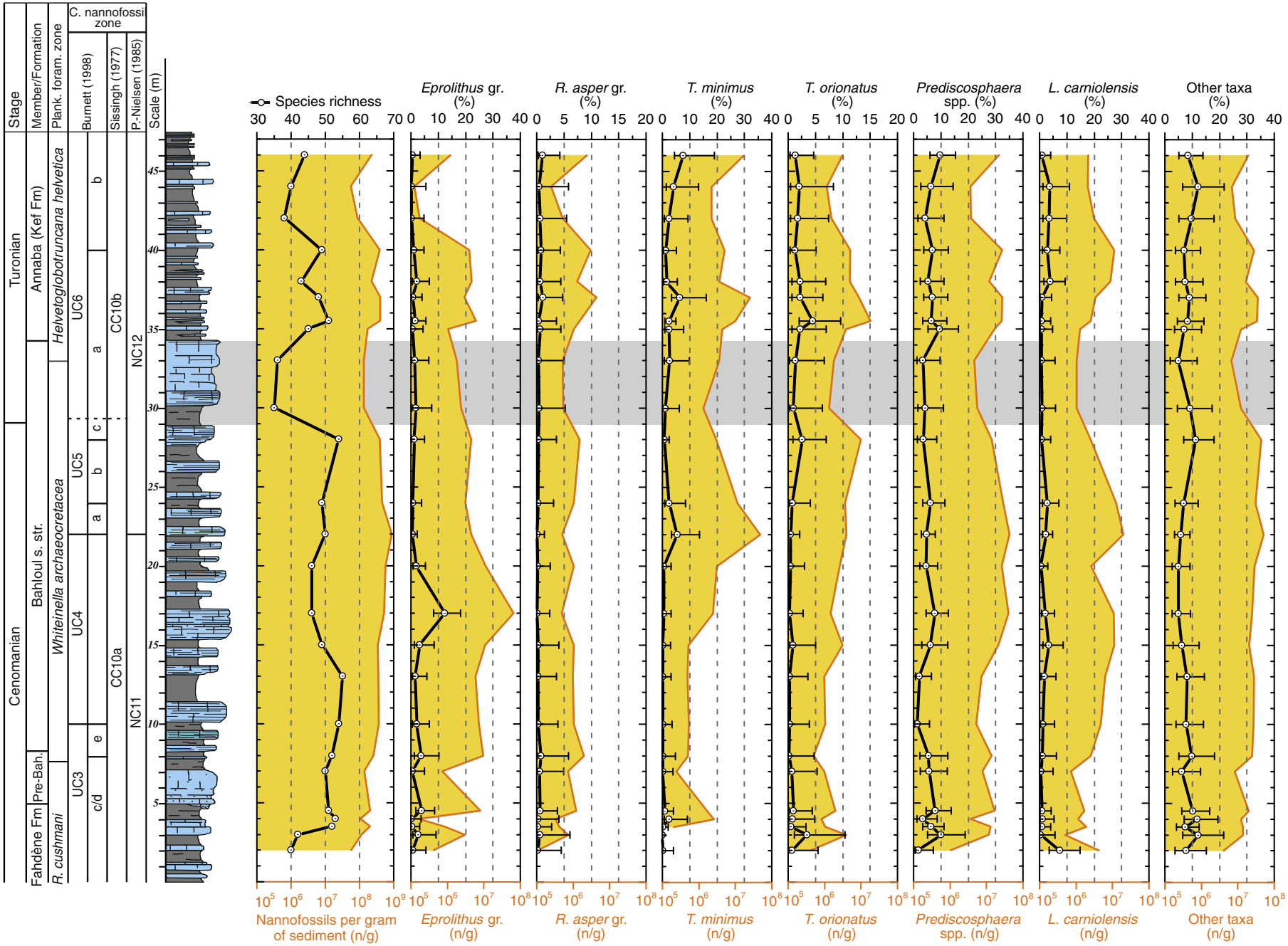

Fig. 7. Fluctuations of selected calcareous nannoplankton taxa throughout the Oued Bahloul section. Absolute abundances (as individuals per gram of sediment) are represented (shaded graphs) in the bottom x-axes, while relative percentage abundances (line and error bars) are represented in the top x-axes. Lithology and biostratigraphy are as in Fig. 2. Shaded horizontal band corresponds to poorly preserved assemblages (see text for details).

Zeugrhabdotus gr. This suggests that *Discorhabdus* probably did not have a preference for nutrients as high as the small *Zeugrhabdotus* gr. and *Biscutum* spp. Alternatively, *Discorhabdus* species may have been more sensitive than other taxa to additional environmental changes (temperature, salinity, pH, redox) that probably set in at the onset and during the OAE2 interval.

5.2. Calcareous nannofossils and palaeotemperature

Rhagodiscus asper and the related *R. splendens* (both included here in *R. asper* gr.) have usually been interpreted as warm-water species whereas the *Eprolithus* gr. (mainly *E. floralis*), is thought to have preferred cool surface waters (Roth and Krumbach, 1986; Mutterlose, 1987; Linnert et al., 2010; Bottini and Mutterlose, 2012; Aguado et al., 2014b). *R. asper* gr. is rare throughout the studied section (Fig. 7), which could be the result of it being a declining taxon (it went extinct in the Turonian), and apparently it does not show clear trends in abundance. *Eprolithus* gr. is also rare, but shows a distinctive peak in abundance in sample OB-17 m, within the lower part of the Bahloul Member (mid-part of the *W. archaeocretacea* Zone, uppermost part of the UC4 Zone). Latest Cenomanian and early Turonian peaks of *E. floralis* and related Polycyclolithaceae have been described from various Atlantic and Tethyan sections (Bralower, 1988; Nederbragt and Fiorentino, 1999; Hardas and Mutterlose, 2007; Melinte-Dobrinescu and Bojar, 2009; Tantawy, 2008; Linnert et al., 2010, 2011). Assuming a cool-water preference of Polycyclolithaceae, *Eprolithus* gr. should not have increased within sample OB-17 m in Oued Bahloul, as $\delta^{18}O_{bulk}$ values remain low (Fig. 2). Furthermore, high abundance values of *Eprolithus* gr. occur in Tethys (85% in Morocco, Tantawy, 2008; 65% in Romania, Melinte-Dobrinescu and Bojar, 2009) whereas North Atlantic values remain low (e.g., 8.5%, Germany: Linnert et al., 2010; 7.8%, England: Linnert et al., 2011). A southward increase of *Eprolithus* gr. frequencies apparently rules out a cool-water preference. Low-nutrient affinity (Linnert et al., 2010) or lower photic zone habitat (Hardas and Mutterlose, 2007) has been instead considered for this taxon. The nutricline is usually located near the base of the seasonal pycnocline (Molfino and McIntyre, 1990; Bolton et al., 2010), within the lower part of the photic zone (MacLaughlin and Carmack, 2010). However, the high proportions of meso- to eutrophic taxa (surface water dwellers) and the evidence of a humid climate (Section 5.5; Soua et al., 2008) during OAE2 in Oued Bahloul suggest that nutricline was displaced to the upper part of the photic zone. These facts apparently contradict a lower photic zone preference for *Eprolithus* gr. As a consequence, the true ecological affinity of the Polycyclolithacea, and the significance of its peaks throughout the late Cenomanian OAE2, are enigmatic and still a matter of debate.

The absence of true cold-water taxa such as *Seribiscutum* and *Repagulum* (Mutterlose and Kessels, 2000; Street and Bown, 2000) and very low abundance/absence of some cool-water taxa as *Ahmuellerella octoradiata* and *Gartnerago segmentatum* (Linnert et al., 2011) indicate a generalized warm surface water environment in Oued Bahloul. *Tranolithus orionatus*, often considered a cool-water species (Bornemann et al., 2005; Hardas and Mutterlose, 2007) is present in a significant (but low) proportion. Its abundance clearly increases throughout the upper part of the Bahloul and Annaba members (Fig. 7), which could be interpreted as the result of progressive cooling. This is also indicated by a progressive increase in the $\delta^{18}O_{bulk}$ values (Fig. 2). A similar, although not identical trend, is observed for the abundance of *Tranolithus minimus* (Fig. 7), suggesting affinity of this taxon for cool waters.

In order to better assess fluctuations in temperature of surface waters, the temperature index (TI) of Bornemann et al. (2005) was adopted and modified by simply not taking into consideration those (cool) taxa that were absent in Oued Bahloul. The results should be considered with caution, due to the very low abundance of the warm-water indicators (*Rhagodiscus* spp.) and the absence/low abundance of cold/cool water taxa. For this reason, smoothing was performed on the obtained values. The fluctuations of TI very broadly mimic the trends observed in the $\delta^{18}O_{bulk}$ curve (Fig. 8). The lower part of the TI curve indicates progressive warming (the same trend indicated by $\delta^{18}O_{bulk}$ values), while progressive cooling may be suggested for the upper part of the TI curve. A distinctive peak in sample OB-35.5 m, indicating a cooling, coincides with a sudden step in the oxygen-isotope curve. Owing to the low-latitude location of the Oued Bahloul (Section 2) and the global greenhouse climate conditions depicted for the OAE2 (Jenkyns, 1999; Voigt et al., 2004; Forster et al., 2007), the fluctuations shown by the adopted TI proxy should rather be considered the result of the change between warmer and less warm (temperate) surface water conditions.

5.3. Other calcareous nannofossil signals

A prominent feature of calcareous nannofossil assemblages of Oued Bahloul section is the presence of significant proportions of holococcoliths (Figs. 3bn–cm, 6), which are especially abundant throughout the Bahloul and basal part of the Annaba members. Holococcoliths are produced during the haploid stages of the heteromorphic haplo-diplontic life cycle common in haptophytes (Billard and Inouye, 2004). Although the factors inducing their secretion are not well established, environmental stress (rapid change in surface water temperature, nutrients, salinity, light) is thought to stimulate heterococcolith-bearing cells to undergo meiosis and release free motile holococcolith-bearing cells (Noël et al., 2004; Mutterlose and Bottini, 2013). The interval enriched in holococcoliths may thus represent further evidence of a marked change in environmental conditions. Enrichments in holococcoliths have been reported from other Cretaceous sediments corresponding to episodes of presumed environmental stress as early Aptian Oceanic Anoxic Event 1a (Mutterlose and Bottini, 2013; Aguado et al., 2014b, c). *Retecapsa* spp. has been ascribed as an euryecious, stress-tolerant taxon (Linnert et al., 2010, 2011), usually related with mesotrophic to eutrophic surface waters (Hardas and Mutterlose, 2007; Linnert and Mutterlose, 2009). Although this taxon is not very common in the studied interval in Oued Bahloul, it shows higher abundances throughout the Pre-Bahloul and Bahloul members, coinciding with the OAE2 interval (Fig. 6).

Both holococcoliths and *Retecapsa* spp. abundances point to high palaeoenvironmental stress conditions in surface waters during deposition of most of the studied interval. These conditions started and were especially intense during deposition of Bahloul Member, although apparently they also prevailed during the sedimentation of the lowermost part of Annaba Member (earliest Turonian).

5.4. Comparison with geochemical proxies

Previous data of geochemical proxies for redox conditions and palaeoproductivity from Oued Bahloul section have been published by Reolid et al. (2015). These authors recorded increasing values of palaeoproductivity proxies, mainly P/Ti, in the Pre-Bahloul Member that were interpreted as relating to enhanced productivity. However, the different productivity indices of fossil nannoplankton (PI and NIP) do not indicate fertilization in the Pre-Bahloul Member. The whole Pre-Bahloul Member was interpreted as a shelf margin wedge by Zagrarni et al. (2008) with record of abundant phosphatic black pebbles, probably related to reworking from other areas that would explain the high P/Ti ratio. Mort et al. (2007a, b) suggested an increase in P-accumulation rates coinciding with the OAE2 and related to increasing surface-water productivity. The enrichment of redox-sensitive elements reported by Reolid et al. (2015) such as Cr, Cu, Mo, Th and U, points to depleted oxygen conditions during deposition of the Pre-Bahloul Member. High values of the U enrichment factor ($U_{EF} = 8.08$) and TOC (2.80 wt.%) point to depleted oxygen conditions in the lower part of the water column at the *R. cushmani*/*W. archaeocretacea* zone boundary, close to the top of the Pre-Bahloul Member. These unfavorable conditions

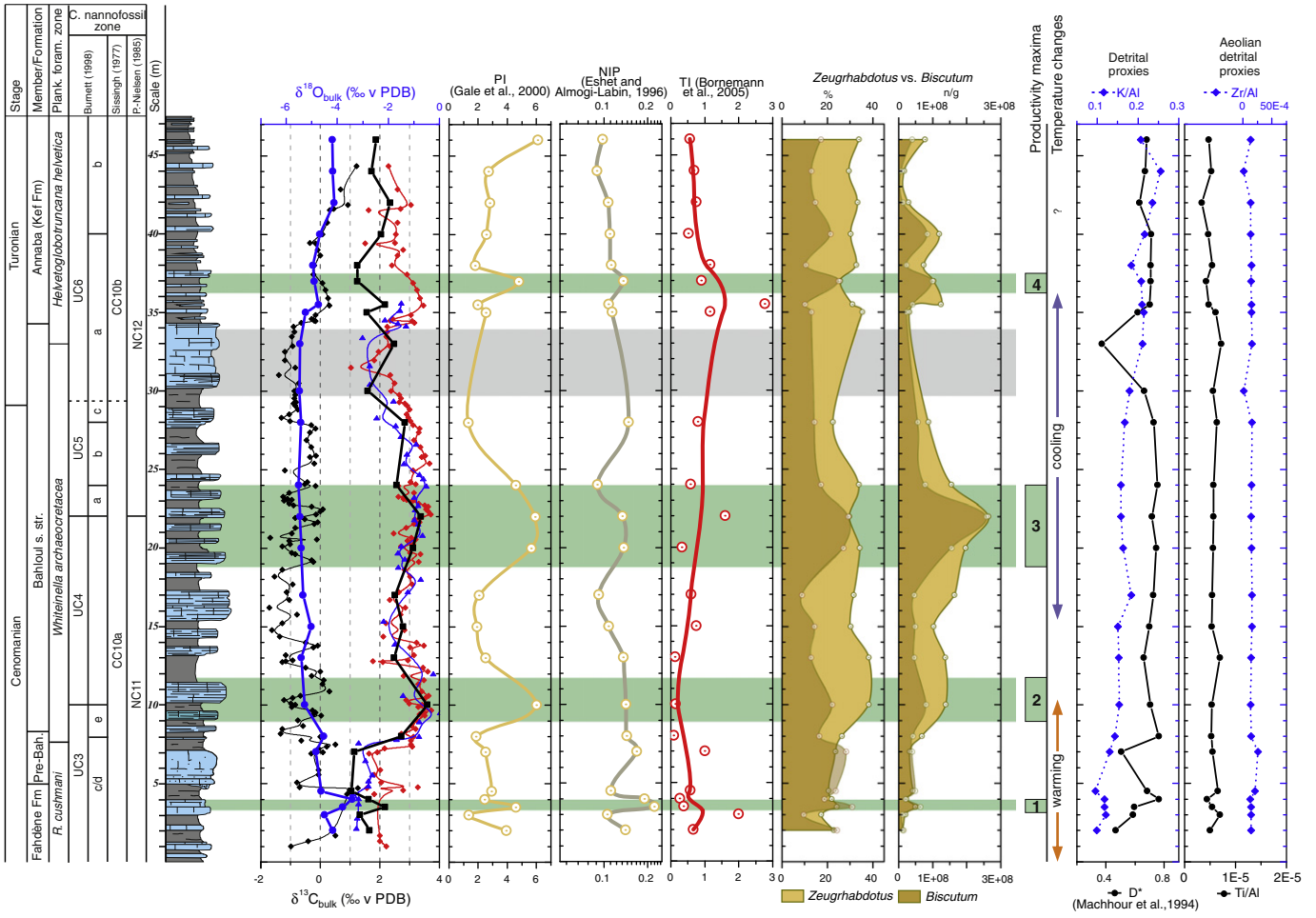

Fig. 8. Fluctuations of productivity (PI: Gale et al., 2000; NIP: Eshet and Almogi-Labin, 1996) and temperature (TI: Bornemann et al., 2005) indices throughout the study interval and comparison with the $\delta^{18}O_{bulk}$, $\delta^{13}C_{bulk}$ curves and the relative and absolute abundances of small *Zeugrhabdotus* gr. vs. *Biscutum* spp. The deduced trends in fertility and temperature are also indicated. For TI curve, an adjacent average smoothing with a window of three points was performed. Data from the poorly preserved interval (grey shaded band) were not considered. At the right side, fluctuations in detrital (D* = circles; K/Al = diamonds) and aeolian detrital (Ti/Al = circles; Zr/Al = diamonds) proxies throughout the section.

caused the disappearance of deep-dweller specialists such as *Rotalipora*. This boundary is related to a transgressive surface (Zagrarni et al., 2008).

The lower part of the Bahloul Member (UC4 Zone) presents an increase in Mo enrichment factor (Mo_{EF}), reaching 12.5, authigenic Mo (Mo_{aut}), Cu/Al, Cr/Al and Ni/Al, with maximum values in sample OB-17 m (Reolid et al., 2015). According to Tribovillard et al. (2012) and Zhou et al. (2012) high Mo_{EF} and Mo_{aut} require the presence of H_2S (euxinic conditions). TOC keeps values around 1.5 wt.% during the $\delta^{13}C$ high values. This is congruent with the benthic barren interval and very low diversity of planktic foraminifera in sample OB-17 m (Reolid et al., 2015) and the presence of euxinic conditions through the OAE2 from other basins (Wang et al., 2001; Scopelliti et al., 2004; Reolid et al., 2016). These results point to poor oxygenation at the sea floor extending upward in the water column during deposition of the lower part of the Bahloul Member, and combined with relatively high TOC and $\delta^{13}C$ values, suggest a major climatic and palaeoceanographic perturbation in a transgressive context (Zagrarni et al., 2008). The abundance of low-oxygen tolerant genera of benthic foraminifera at the base of *W. archaeocretacea* Zone is compatible with the increasing values of TOC (Reolid et al., 2015). The *W. archaeocretacea*/*H. helvetica* zone boundary is characterized by increasing values of redox proxies (Cr/Al, Co/Al, Cu/Al, Ni/Al and Mo_{EF}) coeval with a new peak in opportunists such as benthic foraminifera *Praebulimina*, and planktic foraminifera *Guembelitria* (Reolid et al., 2015). An increase in palaeoproductivity proxies (Sr/Al and P/Ti) occurs in sample OB-35 m (beginning of *H. helvetica* Zone) which, nevertheless, precedes that of calcareous nannoplankton indices of productivity PI and NIP (Fig. 8) at sample OB-37 m.

With regard to detrital proxies, those indicative of eolian input (Ti/Al and Zr/Al) show a uniform stratigraphic distribution (Fig. 8) whereas fluvial detrital proxies such as K/Al present a general increase from the top of the Fahdène Formation to the top of the section. D* ratio shows generally high values (mean ~0.71) compared with typical terrigenous shales (Wedepohl, 1971). The lowest value of D* is recorded in the *W. archaeocretacea*/*H. helvetica* zone boundary, coinciding with the maximum flooding surface (Robaszynski et al., 1990, 1993; Zagrarni et al., 2008), although it increases again at the base of the Kef Formation. The stratigraphic distribution of detrital proxies indicates that the aeolian contribution to the detritic phase remained nearly constant while fluvial input increased during the OAE2.

5.5. Palaeoceanographic implications

Calcareous nannofossil assemblages indicate that moderate to high-fertility surface water conditions predominated during the deposition of the studied interval in the Oued Bahloul section. Reolid et al. (2015) recorded decreasing values of diversity both in planktic and benthic foraminiferal assemblages across the *Rotalipora cushmani*/*Whiteinella archaeocretacea* zone boundary. Some genera of planktic foraminifera disappear, including intermediate to deep-dweller specialists such as *Rotalipora* and *Thalmanninella*, and intermediate-dwellers such as *Praeglobotruncana*. At the same time *Muricohedbergella delrioensis*, a

deep-dweller opportunist adapted to eutrophic conditions (Ando et al., 2010; Reolid et al., 2016) and benthic forms such as buliminids (mainly *Neobulimina*), indicative of oxygen-poor eutrophic conditions proliferated (Koutsoukos et al., 1990; Gebhardt et al., 2004; Sprong et al., 2013). These changes indicate progressively more eutrophic conditions at the beginning of the Bahloul Member.

The highest fertility conditions apparently developed throughout the carbon isotope excursion (CIE), which is the expression of OAE2. These results give support to a productivity-induced instead of a preservation-induced OAE in Oued Bahloul. Data from calcareous nannofossils are compatible with those obtained by Farrimond et al. (1990), based on the analysis of biomarkers from Oued Bahloul section. The proliferation of radiolarians and diatoms reported by Caron et al. (1999) and Soua et al. (2011) in the lower part of the *Whiteinella archaeocretacea* Zone from Oued Bahloul coinciding with the increase of *Planoheterohelix* in dark laminated limestones also points to high productivity during OAE2.

In Oued Bahloul, geochemical proxies give some clues about the probable causes of the eutrophication of the surface waters. The values of the D* geochemical relationship (Machhour et al., 1994) begin to increase throughout the uppermost part of the Fahdène Formation. Increased D* in the organic-rich interval (mean ~0.71 against ~0.55 for typical terrigenous shales; Wedepohl, 1971) indicates an enhanced rate of terrigenous supply during Bahloul Member deposition (Fig. 8). The uniform stratigraphic distribution of K/Al and Ti/Al (Fig. 8), suggests a rather homogeneous nature for the detrital supply. In addition, Ti/Al and Zr/Al ratios, which are regarded as markers for airborne or aeolian detrital supply (Pye, 1987; Scopelliti et al., 2004), do not show significant variations throughout the study interval (Fig. 8). This suggests that aeolian contribution to the detritic phase remained nearly constant. Similar results for geochemical detrital proxies (aeolian and fluvial) have been previously obtained for Oued Bahloul section and adjacent areas (Soua et al., 2008; Soua, 2011). As there are no significant variations in the windblown detrital supply, the enhanced detritic contribution (as suggested by D* and K/Al) recorded throughout the Bahloul Formation should be exclusively interpreted as resulting from increased riverine influx (Soua et al., 2008). A more humid climate could have raised the rate of continental precipitation in the hinterlands adjacent to Oued Bahloul area, increasing fluvial run-off and enhancing detritic contribution to the sediments (Soua et al., 2008). Climatic warming and an enhanced hydrological cycle have been suggested among the triggering factors of the OAE2 episode (Jenkyns, 1999; Voigt et al., 2004; Forster et al., 2007).

As a consequence of enhanced fluvial run-off, increased nutrient input to marine surface waters contributed to eutrophication. This is recorded in calcareous nannofossil assemblages by the increase in abundance of the small *Zeugrhabdotus* gr., *Biscutum* spp., and calcareous nannofossil-derived productivity indices (Fig. 8), and in planktic foraminifera by the disappearance of intermediate and deep-dweller specialists together with proliferation of eutrophic and opportunistic taxa (Reolid et al., 2015). These surface waters, rich in nutrients, were probably less saline that bottom waters, contributing to the development of a freshwater lid and a halocline (e.g., Föllmi, 2012). Plankton consumption of surface-water nutrients increased productivity and organic matter production. As the organic remains sunk towards the bottom waters, their decay contributed to consumption of the dissolved oxygen, generating increasingly dysoxic/anoxic conditions and favoring preservation and accumulation of organic matter. Oxygenation of the bottom waters was probably hindered by the presence of the halocline, which in turn contributed to the development of sluggish circulation and the expansion of anoxia. The expansion of anoxic/dysoxic conditions through the bottom waters was responsible for the minimum diversity values of foraminifera, the local disappearance of benthic forms, the decrease in abundance of deep-dweller opportunist *Muricohedbergella* (Reolid et al., 2015) during the negative CIE (lower part of the *W. archaeocretacea* Zone), while the nutrient-rich surface waters favored intermediate to surface-dweller opportunist *Planoheterohelix* (Caron et al., 2006; Reolid et al., 2015). These changes indicate adverse conditions in deep-water column and bottom waters for foraminifera due to a progressively shallower pycnocline/nutricline and a well-developed oxygen minimum zone close to surface waters.

The burial of large amounts of organic matter throughout the Bahloul Member (and similar organic-rich deposits) was an effective method of carbon sequestration that progressively reduced pCO_2, as suggested by the subsequent relative cooling recorded by calcareous nannofossil assemblages and oxygen isotopes (Fig. 8).

Alternatively, coastal upwelling of deep and denser water masses rich in nutrients or an increased input of windblown dust may also cause surface-water eutrophication (Martin, 1990; Maher et al., 2010). However, both mechanisms need strong and constant winds related to a well-developed planetary windbelt and some climatic models (Hay, 2008; Kiddler and Worsley, 2010) suggest weakened winds during the Cretaceous, and especially throughout the OAE2 interval. This is congruent with our data from aeolian detrital proxies. The only constant winds would have been the easterly ('trade') winds that forced the steady ocean currents of the equatorial system (Pucéat et al., 2005; Hay, 2008; Misumi and Yamanaka, 2008). The dominant direction of the trade winds along the North African continental margin would be from the sea towards the continent, reducing the possibilities of windblown dust fertilization of surface waters in Oued Bahloul area. Furthermore, geochemical proxies in Oued Bahloul section (Ti/Al and Zr/Al) and adjacent areas (Soua, 2011) do not suggest an increase in windblown detrital particles throughout the organic-rich interval. However, intermittent increases of surface-water productivity along the Central Tunisian Platform, induced by some type of coastal upwelling (Soua, 2005) by Ekman transport, related to trade winds and the global ocean circulation pattern (Fig. 9), could not be completely ruled out.

In warmer climate conditions, such as proposed for OAE2, thermoclines are weaker and the position and intensity of pycnocline and ocean circulation is probably controlled by halothermal conditions (Kidder and Worsley, 2010). Moreover, the pycnocline could also be influenced by riverine discharge. According to Reolid et al. (2015) environmental conditions were unfavorable during the negative CIE for the development of deep-dweller planktic foraminifera, probably related to a shallow halocline, surface water fertility and shoaling of the oxygen minimum zone in the water column (lower part of the *W. archaeochetacea* Zone).

High temperatures, slowdown of oceanic circulation and changes in nutrient supply are among the causes for the perturbation of the carbon cycle linked to OAE2 (Jenkyns, 1999; Voigt et al., 2004; Forster et al., 2007; Kiddler and Worsley, 2010). This warming entailed low mixing of surface and deep waters (poor ocean ventilation) and enhanced primary productivity by increasing continental weathering and nutrient input to the ocean. These palaeoenvironmental changes had a significant influence on the composition of foraminiferal (Caron et al., 2006; Reolid et al., 2015) and calcareous nannofossil assemblages. However, nannofossil assemblages from different localities and latitudes were not equally affected. Those from low-latitude localities, such as Oued Bahloul, seem to reflect an increase in nutrient availability, whereas it seems that for assemblages from mid-latitude areas the nutrient content of the surface waters decreased (Fig. 9). The most pronounced OAE2 conditions (high nutrient entry, photic zone euxinia, deposition of organic matter) were limited to the tropical belt (Hardas and Mutterlose, 2007; Tantawy, 2008), whereas the mid-latitudes (Linnert et al., 2010, 2011; Westermann et al., 2010; Linnert and Mutterlose, 2012; Corbett and Watkins, 2013) were less affected (black shales with lower TOC contents, and no euxinia). Increased nutrient availability was apparently limited to the tropical belt and/or mid-southern latitudes (Fig. 9). It is possible that a high consumption of nutrients by tropical phytoplankton, the low recycling of organic matter (accumulation of

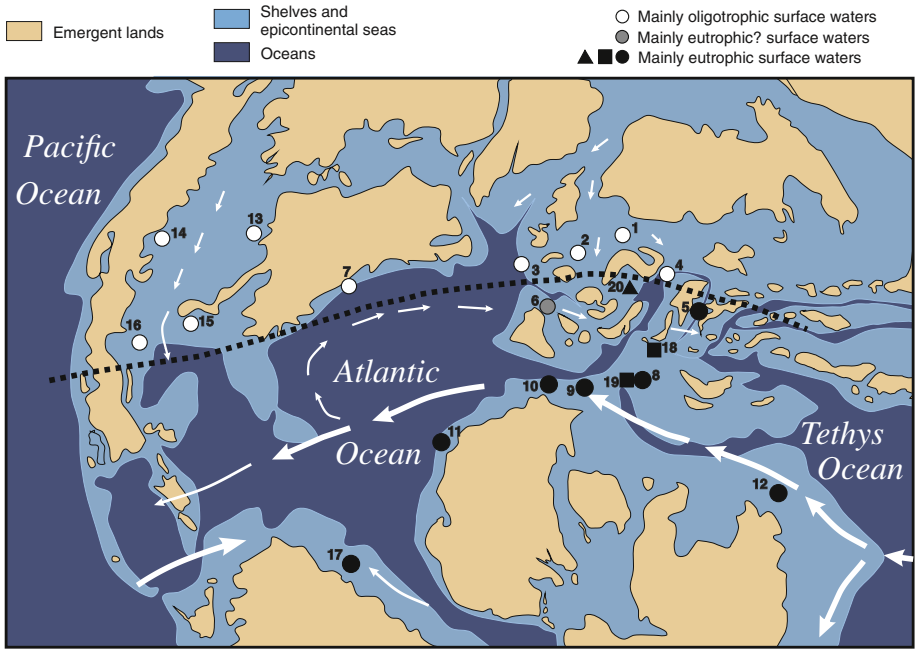

Fig. 9. Palaeogeographic map showing the distribution of sections with calcareous nannofossil assemblages suggesting mainly eutrophic (black dots), mainly oligotrophic (white dots) or mixed oligo-eutrophic intervals of surface waters during the latest Cenomanian. Other sections with proxies suggesting eutrophic surface waters during this time interval are also shown (planktic foraminifera = black squares; geochemical proxies = black triangle). 1, Wunstorf (Linnert et al., 2010); 2 Eastbourne (Gale et al., 2000; Linnert et al., 2011); 3, Goban Spur (Linnert and Mutterlose, 2012); 4, Rehkogelgraben (Pavlishina and Wagreich, 2012); 5, Ohaba-Ponor (Melinte-Dobrinescu and Bojar, 2009); 6, Arobes (Melinte-Dobrinescu et al., 2013); 7, Bass River (Eleson and Bralower, 2005); 8, Novara di Sicilia (Scopelliti et al., 2008); 9, Oued Bahloul (this work); 10, Oued Mellegue (Nederbragt and Fiorentino, 1999); 11, Tazra (Tantawi, 2008); 12, Wadi Feiran (El-Sabbagh et al., 2011); 13, Cuba KS (Eleson and Bralower, 2005; Corbett and Watkins, 2013); 14, Mesa Verde, 15, ACC#1 Core, 16, Fasken "A" #1-H Core (Corbett and Watkins, 2013); 17, Demerara Rise (Hardas and Mutterlose, 2007, Hardas, 2008); 18, Bottaccione, 19, Calabianca-Guidaloca (Coccioni and Luciani, 2005; Scopelliti et al., 2004); 20, Chrummflueschlucht (Westermann et al., 2010). Pattern of surface oceanic currents (arrows) after Pucéat et al. (2005), Misumi and Yamanaka (2008) and Topper et al. (2011). The width and length of the arrows indicate the strength of the currents.

black shales) and sluggish and weakened oceanic circulation have caused the low nutrient availability in mid-latitudes. This general decrease in nutrient availability in mid-latitudes (Fig. 9), contradicts the view of OAE2 as an exclusively productivity-induced oceanic anoxic event suggesting a more complex scenario where alternative models could also be accommodated (e.g., Mort et al., 2007b).

6. Conclusions

The sequence of calcareous nannofossil bioevents recorded in the moderately to well preserved Cenomanian–Turonian assemblages of Oued Bahloul is consistent with most previous studies. The zonations of Sissingh (1977), Perch-Nielsen (1985), and Burnett (1998) were successfully applied and correlated to previously established ammonites and planktic foraminifera zonal scales.

Calcareous nannofossil and foraminiferal assemblages indicate that high-fertility surface-water conditions predominated in Oued Bahloul throughout most of the OAE2 interval. Quantitative analyses of calcareous nannofossil assemblages revealed four episodes of intensified fertility throughout the section, which broadly correlate with maxima in the $\delta^{13}C_{bulk}$ curve. The results of the nannofossil-derived temperature index suggest a warming at the beginning of OAE2 followed by progressive cooling (always within a range of warm temperatures), broadly showing the same trend indicated by $\delta^{18}O_{bulk}$ values. The presence of significant proportions of holococcoliths suggests that high palaeoenvironmental stress conditions prevailed in surface waters through the OAE2 interval and even persisted beyond it.

The enrichment in redox-sensitive elements and low-oxygen tolerant benthic foraminifera indicates that dysoxic conditions both in the deep-water column and at the sea floor were established at the onset of OAE2. Euxinic conditions in deep waters were occasionally reached within the OAE2 interval, as suggested by the disappearance of benthic foraminifera and the record of the highest values of Mo_{EF} and Mo_{aut}.

Geochemical detrital proxies (D* and K/Al versus Ti/Al and Zr/Al ratios) suggest that, in Oued Bahloul, the enhanced detritic contribution through OAE2 should be exclusively interpreted as resulting from increased riverine influx related to a more humid climate. An enhanced fluvial run-off increased nutrient input to marine surface waters contributing to eutrophication. Plankton consumption of surface-water nutrients increased organic matter production, whose decay contributed to the decrease of dissolved oxygen in bottom waters, generating increasingly dysoxic/anoxic conditions and favoring accumulation and preservation of organic matter.

Although calcareous nannoplankton assemblages from low-latitude locations, such as those of Oued Bahloul, reflect an increase in nutrient availability through OAE2, the nutrient content of the surface waters decreased in those from mid-latitude areas.

Acknowledgments

The authors wish to thank Dalila Zaghbib-Turki and Mohamed Soua, who helped us sample the Oued Bahloul section and A. Carrillo for her help with the processing of calcareous nannofossil micropalaeontological samples. We thank K. Föllmi and M. Corbett for reviews. This work is a contribution of the research projects CGL2011-23759, CGL2014-52546-P, CGL2014-55274-P and CGL2014-58794-P of the Spanish Ministry of Science and Technology (FEDER funds), and RNM-200 (Junta de Andalucía).

Appendix A. Taxonomic appendix

Family Kamptneriaceae Bown and Hampton, 1997 *in* Bown and Young, 1997.
Genus *Gartnerago* Bukry, 1969.
Gartnerago aenigma (Burnett, 1997) comb. nov.
Basyonim: *Staurolithites? aenigma* Burnett, 1997, p. 139, pl. 1, Fig. 1a–b.

(1a–1b = holotype). Burnett, J.A., 1997. New species and new combinations of Cretaceous nannofossils and a note on the origin of *Petrarhabdus* (Deflandre) Wind and Wise. J. Nannoplankton Res. 19, 133–146.
Remarks: the complex rim (dark outer cycle, bright median cycle and dark inner cycle) and central area structures of this species resemble those of *Gartnerago* more than those of *Staurolithites*. A very similar taxon is *Gartnerago margaritatus* Blair and Watkins, 2009, from the uppermost Coniacian to Lower Santonian of the Western Interior Basin in the USA.

Appendix B. Supplementary data

Table with the results of the quantitative study and alphabetical list of calcareous nannofossil taxa identified. Supplementary data associated with this article can be found in the online version, at http://dx.doi.org/10.1016/j.palaeo.2016.07.016.

References

Accarie, H., Robaszynski, F., Amédro, F., Caron, M., Zagrarni, M.F., 2000. Stratigraphie événementielle au passage Cénomanien-Turonien dans le secteur occidental de la plate-forme de la Tunisie centrale (Formation Bahloul, région de Kalaat Senan). Ann. Mines Géol. Tunis 40, 63–80.

Aguado, R., 2012. Two new Cretaceous calcareous nannofossils from SE Spain and Tunisia. J. Nannoplankton Res. 32, 53–57.

Aguado, R., O'Dogherty, L., Sandoval, J., 2008. Fertility changes in surface waters during the Aalenian (mid Jurassic) of the Western Tethys as revealed by calcareous nannofossils and carbon-cycle perturbations. Mar. Micropaleontol. 68, 268–285.

Aguado, R., Company, M., O'Dogherty, L., Sandoval, J., Tavera, J.M., 2014a. Late Hauterivian–early Barremian calcareous nannofossil biostratigraphy, palaeoceanography, and stable isotope record in the Subbetic domain (southern Spain). Cretac. Res. 49, 105–124.

Aguado, R., de Gea, G.A., Castro, J.M., O'Dogherty, L., Quijano, M.L., Naafs, B.D.A., Pancost, R.D., 2014b. Late Barremian–early Aptian dark facies of the Subbetic (Betic Cordillera, southern Spain): calcareous nannofossil quantitative analyses, chemostratigraphy and palaeoceanographic reconstructions. Palaeogeogr. Palaeoclimatol. Palaeoecol. 395, 198–221.

Aguado, R., de Gea, G.A., O'Dogherty, L., 2014c. Integrated biostratigraphy (calcareous nannofossils, planktonic foraminifera, and radiolaria) of an uppermost Barremian–lower Aptian pelagic succession in the Subbetic Basin (southern Spain). Cretac. Res. 51, 153–173.

Amédro, F., Accarie, H., Robaszynski, F., 2005. Position de la limite Cénomanien-Turonien dans la Formation Bahloul de Tunisie centrale: apports intégrés des ammonites et des isotopes du carbone ($\delta^{13}C$). Eclogae Geol. Helv. 98, 151–167.

Ando, A., Huber, B.T., MacLeod, K.G., 2010. Depth-habitat reorganization of planktonic foraminifera across the Albian/Cenomanian boundary. Paleobiology 36, 357–373.

Billard, C., Inouye, I., 2004. What is new in coccolithophore biology? In: Thierstein, H.R., Young, J.R. (Eds.), Coccolithophores. From Molecular Processes to Global Impact. Springer-Verlag, Berlin, pp. 1–29

Blair, S.A., Watkins, D.K., 2009. High-resolution calcareous nannofossil biostratigraphy for the Coniacian/Santonian Stage boundary, Western Interior Basin. Cretac. Res. 30, 367–384.

Blakey, R., 2005. Global paleogeography. http://jan.ucc.nau.edu/~rcb7/globaltext2.html.

Bolton, C.T., Gibbs, S.J., Wilson, P.A., 2010. Evolution of nutricline dynamics in the equatorial Pacific during the late Pliocene. Paleoceanography 25, PA1207. http://dx.doi.org/10.1029/2009PA001821.

Bornemann, A., Pross, J., Reichelt, K., Herrle, J.O., Hemleben, C., Mutterlose, J., 2005. Reconstruction of short-term palaeoceanographic changes during the formation of the Late Albian 'Niveau Breistroffer' black shales (Oceanic Anoxic Event 1d, SE France). J. Geol. Soc. Lond. 162, 623–639.

Bottini, C., Mutterlose, J., 2012. Integrated stratigraphy of Early Aptian black shales in the Boreal Realm: calcareous nannofossil and stable isotope evidence for global and regional processes. Newsl. Stratigr. 45, 115–137.

Bown, P.R., 1998. Calcareous nannofossil biostratigraphy. British Micropalaeontological Society Publication Series, first ed. Chapman and Hall, London (314 pp.).

Bown, P.R., Young, J.R., 1997. Mesozoic calcareous nannoplankton classification. J. Nannoplankton Res. 19, 21–36.

Bralower, T.J., 1988. Calcareous nannofossil biostratigraphy and assemblages of the Cenomanian-Turonian boundary interval: implications for the origin and timing of oceanic anoxia. Paleoceanography 3, 275–316.

Bukry, D., 1969. Upper Cretaceous coccoliths from Texas and Europe. University of Kansas Paleontological Contributions 51, 1–79.

Burnett, J.A., 1997. New species and new combinations of Cretaceous nannofossils and a note on the origin of *Petrarhabdus* (Deflandre) Wind and Wise. J. Nannoplankton Res. 19, 133–146.

Burnett, J.A., 1998. Upper Cretaceous. In: Bown, P.R. (Ed.), Calcareous Nannofossil Biostratigraphy, 1 ed. Chapman & Hall, London, pp. 132–199.

Caron, M., Robaszynski, F., Amédro, F., Baudin, F., Deconinck, J.F., Hochli, P., Von Salis-Perch Nielsen, K., Tribovillard, N., 1999. Estimation de la durée de l'événement anoxique global au passage Cénomanien-Turonien. Approche cyclostratigraphique dans la Formation Bahloul en Tunisie centrale. Bull. Soc. Geol. Fr. 170, 145–160.

Caron, M., Dall'Agnolo, S., Accaire, H., Barrera, E., Kauffman, E.G., Amédro, F., Robaszynski, F., 2006. High-resolution stratigraphy of the Cenomanian–Turonian boundary interval at Pueblo (USA) and wadi Bahloul (Tunisia): stable isotope and bio-events correlation. Geobios 39, 171–200.

Chester, R., Baxter, G.B., Behairy, A.K.A., Connor, K., Cross, D., Elderfield, H., Padgham, R.C., 1977. Soil-sized eolian dusts from the lower troposphere of the Eastern Mediterranean Sea. Mar. Geol. 24, 201–217.

Coccioni, R., Luciani, V., 2005. Planktonic foraminifers across the Bonarelli Event (OAE2, latest Cenomanian): the Italian record. Palaeogeogr. Palaeoclimatol. Palaeoecol. 224, 167–185.

Corbett, M.J., Watkins, D.K., 2013. Calcareous nannofossil paleoecology of the mid-Cretaceous Western Interior Seaway and evidence of oligotrophic surface waters during OAE2. Palaeogeogr. Palaeoclimatol. Palaeoecol. 392, 510–523.

Corfield, R.M., 1995. An introduction of the techniques, limitations and landmarks of carbonate oxygen isotope palaeothermometry. In: Boscence, D.W.J., Allison, P.A. (Eds.), Marine Palaeoenvironmental Analysis From Fossils. Geological Society Special Publication, pp. 27–42.

Duchamp-Alphonse, S., Gardin, S., Fiet, N., Bartolini, A., Blamart, D., Pagel, M., 2007. Fertilization of the northwestern Tethys (Vocontian basin, SE France) during Valanginian carbon isotope perturbation: evidence from calcareous nannofossils and trace element data. Palaeogeogr. Palaeoclimatol. Palaeoecol. 243, 132–151.

Eleson, J.W., Bralower, T.J., 2005. Evidence of changes in surface water temperature and productivity at the Cenomanian/Turonian Boundary. Micropaleontology 51, 319–332.

El-Sabbagh, A., Tantawy, A.A.A.M., Keller, G., Khozyem, H., Spangenberg, J., Adatte, T., Gertsch, B., 2011. Stratigraphy of the Cenomanian-Turonian Oceanic Anoxic Event OAE2 in shallow shelf sequences of NE Egypt. Cretac. Res. 32, 705–722.

Erba, E., 1992. Middle Cretaceous calcareous nannofossils from the Western Pacific (Leg 129): evidence for paleoequatorial crossings. Proc. ODP Sci. Results 129, 189–201.

Erba, E., Bottini, C., Faucher, G., 2013. Cretaceous large igneous provinces: the effects of submarine volcanism on calcareous nannoplankton. Mineral. Mag. 77, 1044.

Erbacher, J., Huber, B.T., Norris, R.D., Markey, M., 2001. Increased thermohaline stratification as a possible cause for an ocean anoxic event in the Cretaceous period. Nature 409, 325–327.

Eshet, Y., Almogi-Labin, A., 1996. Calcareous nannofossils as paleoproductivity indicators in Upper Cretaceous organic-rich sequences in Israel. Mar. Micropaleontol. 29, 37–61.

Farrimond, P., Eglinton, G., Brassell, S.C., 1990. The Cenomanian/Turonian anoxic event in Europe: an organic geochemical study. Mar. Pet. Geol. 7, 75–89.

Fisher, R.A., Corbet, A.S., Williams, C.B., 1943. The relation between the number of species and the number of individuals in a random sample of an animal population. J. Anim. Ecol. 12, 42–58.

Föllmi, K.B., 2012. Early Cretaceous life, climate and anoxia. Cretac. Res. 35, 230–257.

Forster, A., Schouten, S., Moriya, K., Wilson, P.A., Sinninghe-Damsté, J.S., 2007. Tropical warming and intermittent cooling during the Cenomanian–Turonian Oceanic Anoxic Event 2: sea surface temperature from the equatorial Atlantic. Paleoceanography 22, PA1219. http://dx.doi.org/10.1029/2006PA001349,2007.

Gale, A.S., Smith, A.B., Monks, N.E.A., Young, J.A., Howard, A., Wray, D.S., Huggett, J.M., 2000. Marine biodiversity through the Late Cenomanian–Early Turonian: palaeoceanographic controls and sequence stratigraphic biases. J. Geol. Soc. Lond. 157, 745–757.

Gebhardt, H., Kuhnt, W., Holbourn, A., 2004. Foraminiferal response to sea level change, organic flux and oxygen deficiency in the Cenomanian of the Tarfaya Basin, southern Morocco. Mar. Micropaleontol. 53, 133–157.

Geisen, M., Bollmann, J., Herrle, J.O., Mutterlose, J., Young, J.R., 1999. Calibration of the random settling technique for calculation of absolute abundances of calcareous nannoplankton. Micropaleontology 45, 437–442.

Hammer, Ø., Harper, D.A.T., Ryan, P.D., 2001. PAST: Paleontological Statistics software package for education and data analysis. Palaeontol. Electron. 4, 1–9.

Handoh, I.C., Lenton, T.M., 2003. Periodic mid-Cretaceous oceanic anoxic events linked by oscillations of the phosphorous and oxygen biogeochemical cycles. Glob. Biogeochem. Cycles 17 http://dx.doi.org/10.1029/2003GB002039.

Hardas, P., 2008. The response of calcareous nannofossils to Oceanic Anoxic Event 2 and the Middle Cenomanian Event in the tropical Atlantic: biostratigraphy and palaeoceanographic implications (PhD Thesis) Fakultät für Geowissenschaften. Ruhr-Universität (133 pp.).

Hardas, P., Mutterlose, J., 2007. Calcareous nannofossil assemblages of Oceanic Anoxic Event 2 in the equatorial Atlantic: evidence of an eutrophication event. Mar. Micropaleontol. 66, 52–69.

Hardenbol, J., Thierry, J., Farley, M.B., Jacquin, T., de Graciansky, P.C., Vail, P.R., 1998. Mesozoic and Cenozoic Sequence chronostratigraphic framework of European Basins. In: Graciansky, P.C., Hardenbol, J., Jacquin, T., Vail, P.R. (Eds.), Mesozoic and Cenozoic Sequence Stratigraphy of European Basins. SEPM Sp. Publ. vol. 60, pp. 3–13.

Hay, W.W., 2008. Evolving ideas about the Cretaceous climate and ocean circulation. Cretac. Res. 29, 725–753.

Herrle, J.O., 2003. Reconstructing nutricline dynamics of mid-Cretaceous oceans: evidence from calcareous nannofossils from the Niveau Paquier black shale (SE France). Mar. Micropaleontol. 47, 307–321.

Heslop, D., De Schepper, S., Proske, U., 2011. Diagnosing the uncertainty of taxa relative abundances derived from count data. Mar. Micropaleontol. 79, 114–120.

Huber, B.T., Norris, R.D., McLeod, K.G., 2002. Deep-sea paleotemperature record of extreme warmth during the Cretaceous. Geology 30, 123–126.

Jenkyns, H.C., 1999. Mesozoic anoxic events and paleoclimate. Zbl. Geol. Paläont. Teil I, H 7–9, 943–949.
Kennedy, W.J., Gale, A.S., Bown, P.R., Caron, M., Davey, R.J., Gröcke, D.R., Wray, D.S., 2000. Integrated stratigraphy across the Aptian-Albian boundary in the Marnes Bleues, at the Col de Pré-Guittard, Arnayon (Drôme), and at Tartonne (Alpes-de-Haute-Provence), France: a candidate Global Boundary Stratotype Section and Boundary Point for the base of the Albian Stage. Cretac. Res. 21, 591–720.
Kessels, K., Mutterlose, J., Ruffell, A., 2003. Calcareous nannofossils from late Jurassic sediments of the Volga Basin (Russian Platform): evidence for productivity-controlled black shale deposition. Int. J. Earth Sci. (Geologische Runschau) 92, 743–757.
Kidder, D.L., Worsley, T.R., 2010. Phanerozoic Large Igneous Provinces (LIPs), HEATT (Haline Euxinic Acidic Thermal Transgression) episodes, and mass extinctions. Palaeogeogr. Palaeoclimatol. Palaeoecol. 295, 162–191.
Koutsoukos, E.A.M., Leary, P.N., Hart, M.B., 1990. Latest Cenomanian-earliest Turonian low-oxygen tolerant benthonic foraminifera: a case-study from the Serpige basin (NE Brazil) and the western Anglo-Paris basin (southern England). Palaeogeogr. Palaeoclimatol. Palaeoecol. 77, 145–177.
Lees, J.A., 2007. New and rarely reported calcareous nannofossils from the Late Cretaceous of coastal Tanzania: outcrop samples and Tanzania Drilling Project Sites 5, 9 and 15. J. Nannoplankton Res. 29, 39–65.
Lees, J.A., Bown, P.R., Mattioli, E., 2005. Problems with proxies? Cautionary tales of calcareous nannofossil paleoenvironmental indicators. Micropaleontology 51, 333–343.
Linnert, C., Mutterlose, J., 2009. Evidence of increasing surfacewater oligotrophy during the Campanian–Maastrichtian boundary interval: Calcareous nannofossils from DSDP Hole 390A (Blake Nose). Mar. Micropaleontol. 73, 26–36.
Linnert, C., Mutterlose, J., 2012. Biometry of Cenomanian–Turonian placoliths: a proxy for changes of fertility and surface-water temperature? Lethaia 46, 82–97.
Linnert, C., Mutterlose, J., Erbacher, J., 2010. Calcareous nannofossils of the Cenomanian/Turonian boundary interval from the Boreal Realm (Wunstorf, northwest Germany). Mar. Micropaleontol. 74, 38–58.
Linnert, C., Mutterlose, J., Mortimore, R.N., 2011. Calcareous nannofossils from Eastbourne (southeastern England) and the paleoceanography of the Cenomanian-Turonian boundary interval. PALAIOS 26, 298–313.
Machhour, L., Philip, J., Oudin, J.L., 1994. Formation of laminate deposits in anaerobic–dysaerobic marine environments. Mar. Geol. 117, 287–302.
MacLaughlin, F.A., Carmack, E.C., 2010. Deepening of the nutricline and chlorophyll maximum in the Canada Basin interior, 2003–2009. Geophys. Res. Lett. 37, L24602. http://dx.doi.org/10.1029/2010GL045459.
Maher, B.A., Prospero, J.M., Mackie, D., Gaiero, D., Hesse, P.P., Balkanski, Y., 2010. Global connections between eolian dust, climate and ocean biogeochemistry at the present day and at the last glacial maximum. Earth Sci. Rev. 99, 61–97.
Martin, J.H., 1990. Glacial-interglacial CO_2 change: the iron hypothesis. Paleoceanography 5, 1–13. http://dx.doi.org/10.1029/PA005i001p00001.
Melinte-Dobrinescu, M.C., Bojar, A.-V., 2009. Biostratigraphic and isotopic record of the Cenomanian–Turonian deposits in the Ohaba-Ponor section (SW Haţeg, Romania). Cretac. Res. 29, 1024–1034.
Melinte-Dobrinescu, M.C., Bernárdez, E., Kaiho, K., Lamolda, M.A., 2013. 2013. Cretaceous Oceanic Anoxic Event 2 in the Arobes section, northern Spain: nannofossil fluctuations and isotope events. Geol. Soc. Lond. Spec. Publ. 382, 63–84.
Misumi, K., Yamanaka, Y., 2008. Ocean anoxic events in the mid-Cretaceous simulated by a 3-D biogeochemical general circulation model. Cretac. Res. 29, 893–900.
Molfino, B., McIntyre, A., 1990. Precessional forcing of nutricline dynamics in the Equatorial Atlantic. Science 249, 766–769.
Möller, C., Mutterlose, J., 2014. Middle Hauterivian biostratigraphy and palaeoceanography of the Lower Saxony Basin (Northwest Germany). Z. Dt. Ges. Geowiss. (German J. Geosci.) 165, 501–520.
Monteiro, F.M., Pancost, R.D., Ridwell, A., Donnadieu, Y., 2012. Nutrients as the dominant control on the spread of anoxia and euxinia across the Cenomanian-Turonian oceanic anoxic event (OAE2): model-data comparison. Paleoceanography 27, PA4209. http://dx.doi.org/10.1029/2012PA002351.
Mort, M., Adatte, T., Föllmi, K.B., Keller, G., Steinmann, P., Matera, V., Berner, Z., Stüben, D., 2007a. Phosphorous and the roles of productivity and nutrient recycling during oceanic event 2. Geology 35, 483–486.
Mort, H.P., Jacquat, O., Adatte, T., Steinmann, P., Föllmi, K.B., Matera, V., Berner, Z., Stüben, D., 2007b. The Cenomanian/Turonian anoxic event at the Bonarelli Level in Italy and Spain: enhanced productivity and/or better preservation? Cretac. Res. 28, 597–612.
Mutterlose, J., 1987. Calcareous nannofossils and belemnites as warmwater indicators from the NW-German Middle Aptian. Geol. Jb. A96, 293–313.
Mutterlose, J., 1991. Das Verteilungs- und Migrationsmuster des kalkigen Nannoplanktons in der borealen Unter-Kreide (Valangin-Apt) NW-Deutschlands. Palaeontographica B221, 27–152.
Mutterlose, J., Bottini, C., 2013. Early Cretaceous chalks from the North Sea giving evidence for global change. Nat. Commun. 4, 1686. http://dx.doi.org/10.1038/ncomms2698.
Mutterlose, J., Kessels, K., 2000. Early Cretaceous calcareous nannofossils from high latitudes: implications for palaeobiogeography and palaeoclimate. Palaeogeogr., Palaeoclimatol., Palaeoecol. 160, 347–372.
Nederbragt, A.J., Fiorentino, A., 1999. Stratigraphy and palaeoceanography of the Cenomanian-Turonian Boundary Event in Oued Mellegue, north-western Tunisia. Cretac. Res. 20, 47–62.
Noël, M., Kawachi, M., Inouye, I., 2004. Induced dimorphic life cycle of a coccolithophorid, *Calyptrosphaera sphaeroidea* (prymnesiophyceae, haptophyta). J. Phycol. 40, 112–129.
Pagano, R., 2013. Understanding Statistics in the Behavioral Sciences. 10th ed. Cengage Learning, Wadsworth, CA (640 pp.).
Pavlishina, P., Wagreich, M., 2012. Biostratigraphy and paleoenvironments in a northwestern Tethyan Cenomanian-Turonian boundary section (Austria) based on palynology and calcareous nannofossils. Cretac. Res. 38, 103–112.
Perch-Nielsen, K., 1985. Mesozoic calcareous nannofossils. In: Bolli, H.M., Saunders, J.B., Perch-Nielsen, K. (Eds.), Plankton Stratigraphy. Cambridge University Press, Cambridge, pp. 329–426.
Pucéat, E., Lécuyer, C., Reisberg, L., 2005. Neodymium isotope evolution of NW Tethyan upper ocean waters throughout the Cretaceous. Earth Planet. Sci. Lett. 236, 705–720.
Pye, K., 1987. Aeolian Dust and Dust Deposits. Academic Press, London (334 pp.).
Reolid, M., Rodríguez-Tovar, F.J., Marok, A., Sebane, A., 2012. The Toarcian oceanic anoxic event in the Western Saharan Atlas, Algeria (North African paleomargin): role of anoxia and productivity. Geol. Soc. Am. Bull. 124, 1646–1664.
Reolid, M., Sánchez-Quiñónez, C.A., Alegret, L., Molina, E., 2015. Palaeoenvironmental turnover across the Cenomanian-Turonian transition in Oued Bahloul, Tunisia: foraminifera and geochemical proxies. Palaeogeogr. Palaeoclimatol. Palaeoecol. 417, 491–510.
Reolid, M., Sánchez-Quiñónez, C.A., Alegret, L., Molina, E., 2016. The biotic crisis across the Oceanic Anoxic Event 2: palaeoenvironmental inferences based on foraminifera and geochemical proxies from the South Iberian Palaeomargin. Cretac. Res. 60, 1–27.
Robaszynski, F., Caron, M., Dupuis, C., Amédro, F., González-Donoso, J.M., Linares, D., Hardenbol, J., Gartner Jr., S., Calandra, F., Deloffre, R., 1990. A tentative integrated stratigraphy in the Turonian of central Tunisia: formations, zones and sequential stratigraphy in the Kalaat Senan area. Bull. Centres Rech. Explor. Prod. Elf-Aquitaine 14, 21–384.
Robaszynski, F., Caron, M., Amédro, F., Dupuis, C., Hardenbol, J., González-Donoso, J.M., Linares, D., Gartner, S., 1993. Le Cénomanien de la región de Kalaat Senan (Tunisie Centrale): Litho-biostratigraphie et interprétation séquentielle. Rev. Paléobiol. 12, 351–505.
Rost, B., Riebesell, U., 2004. Coccolithophores and the biological pump: responses to environmental changes. In: Thierstein, H.R., Young, J.R. (Eds.), Coccolithophores. From Molecular Processes to Global Impact. Springer-Verlag, Berlin, pp. 99–125.
Roth, P.H., Bowdler, J.L., 1981. Middle Cretaceous nannoplankton biogeography of the Atlantic ocean. SEPM Spec. Publ. 32, 517–546.
Roth, P.H., Krumbach, K.R., 1986. Middle Cretaceous calcareous nannofossil biogeography and presevation in the Atlantic and Indian oceans: implications for paleoceanography. Mar. Micropaleontol. 10, 235–266.
Roth, P.H., Thierstein, H.R., 1972. Calcareous nannoplankton: Leg 14 of the Deep Sea Drilling Project. Initial Rep. Deep Sea Drill. Proj. 14, 421–485.
Sarmiento, J.L., Herbert, T.D., Toggweiler, J.R., 1988. Causes of anoxia in the world ocean. Glob. Biogeochem. Cycles 2, 115–128.
Scopelliti, G., Bellanca, A., Coccioni, R., Luciani, V., Neri, R., Baudin, F., Chiari, M., Marcucci, M., 2004. High-resolution geochemical and biotic records of the Tethyan 'Bonarelli Level' (OAE2, latest Cenomanian) from the Calabianca–Guidaloca composite section, northwestern Sicily, Italy. Palaeogeogr. Palaeoclimatol. Palaeoecol. 208, 293–317.
Scopelliti, G., Bellanca, A., Erba, E., Jenkyns, H.C., Neri, R., Tamagnini, P., Luciani, V., Masetti, D., 2008. Cenomanian–Turonian carbonate and organic-carbon isotope records, biostratigraphy and provenance of a key section in NE Sicily, Italy: palaeoceanographic and palaeogeographic implications. Palaeogeogr. Palaeoclimatol. Palaeoecol. 265, 59–77.
Shannon, C.C., Weaver, W., 1949. The Mathemathical Theory of Communication. University of Illinois Press, Urbana, Illinois (125 pp.).
Simpson, G.G., 1960. Notes on the measurement of faunal resemblance. Amer. J. Sci. 258A, 300–311.
Sissingh, W., 1977. Biostratigraphy of Cretaceous calcareous nannoplankton. Geol. Mijnb. 56, 37–65.
Soua, M., 2005. Biostratigraphie de haute résolution des foraminifères planctoniques du passage Cénomanien Turonien et impact de l'événement anoxique EAO-2 sur ce groupe dans la marge sud de la Téthys, exemple régions de Jerissa et Bargou. Univ. Tunis El Manar, Mémoir de Mastère (169 pp.).
Soua, M., 2011. Productivity and bottom water redox conditions at the Cenomanian-Turonian Oceanic Anoxic Event in the southern Tethyan margin, Tunisia. Rev. Med. Environ. 4, 653–664.
Soua, M., Zaghbib-Turki, D., Trivobillard, N., 2008. Riverine influxes, warm and humid climatic conditions during the latest Cenomanian-Early Turonian Bahloul deposition. Proc. 11th Tunisian Petroleum Exploration and Production conference. ETAP Mem. 27, 194–200.
Soua, M., Zaghbib-Turki, D., Ben Jemia, H., Smaoui, J., Boukadi, A., 2011. Geochemical record of the Cenomanian-Turonian Anoxic Event in Tunisia: is it correlative and isochronous to the biotic signal? Acta Geol. Sin. 85, 801–840.
Sprong, J., Kouwenhoven, T.J., Bornemann, A., Dupuis, C., Speijer, R.P., Stassen, P., Steurbaut, E., 2013. In search of the Latest Danian Event in a paleobathymetric transect off Kasserine Island, north-central Tunisia. Palaeogeogr. Palaeoclimatol. Palaeoecol. 379, 1–16.
Street, C., Bown, P.R., 2000. Palaeobiogeography of Early Cretaceous (Berriasian-Barremian) calcareous nannoplankton. Mar. Micropaleontol. 39, 265–291.
Tantawy, A.A.A.M., 2008. Calcareous nannofossil biostratigraphy and paleoecology of the Cenomanian–Turonian transition in the Tarfaya Basin, southern Morocco. Cretac. Res. 29, 995–1007.
Thierstein, H.R., 1980. Selective dissolution of Late Cretaceous and earliest Tertiary calcareous nannofossils: experimental evidence. Cretac. Res. 2, 165–176.
Topper, R.P.M., Trabucho Alexandre, J., Tuenter, E., Meijer, P.T., 2011. A regional ocean circulation model for the mid-Cretaceous North Atlantic Basin: implications for black shale formation. Clim. Past 7, 277–297.

Trivobillard, N., Algeo, T.J., Baudin, F., Riboulleau, A., 2012. Analysis of marine environmental conditions based on molybdenum-uranium covariation – applications to Mesozoic paleoceanography. Chem. Geol. 324–325, 46–58.

Tsandev, I., Slomp, C.P., 2009. Modeling phosphorous cycling and carbon burial during Cretaceous Oceanic Anoxic Events. Earth Planet. Sci. Lett. 286, 71–79.

Voigt, S., Gale, A.S., Flögel, S., 2004. Midlatitude shelf seas in the Cenomanian–Turonian greenhouse world: temperature evolution and North Atlantic circulation. Paleoceanography 19, PA4020. http://dx.doi.org/10.1029/2004PA001015.

Wang, C.S., Hu, X.M., Jansa, L., Wan, X.Q., Tao, R., 2001. The Cenomanian-Turonian anoxic event in southern Tibet. Cretac. Res. 22, 481–490.

Wedepohl, K.H., 1971. Environmental influences on the chemical composition of shales and clays. In: Ahrens, L.H., Press, F., Runcorn, S.K., Urey, H.C. (Eds.), Physics and Chemistry of the Earth. Pergamon, Oxford, pp. 305–333.

Westermann, S., Caron, M., Fiet, N., Fleitmann, D., Matera, V., Adatte, T., Föllmi, K.B., 2010. Evidence for oxic conditions during Oceanic Anoxic Event 2 in the northern Tethyan pelagic realm. Cretac. Res. 31, 500–514.

Zagrarni, M.F., Negra, M.H., Hanini, A., 2008. Cenomanian–Turonian facies and sequence stratigraphy, Bahloul Formation. Tunisia. Sediment. Geol. 204, 18–35.

Zhou, L., Wignall, P.B., Su, J., Feng, Q., Xie, S., Zhao, L., Huang, J., 2012. U/Mo ratios and $\delta^{98/95}$Mo as local and global redox proxies during mass extinction events. Chem. Geol. 324–325, 99–197.